Recent Progress in Time-Resolved Biosensing and Bioimaging Based on Lanthanide-Doped Nanoparticles

Qinqin Ma, Jie Wang, Zhiheng Li, Xiaobo Lv, Ling Liang, and Quan Yuan*

Luminescent nanomaterials have attracted great attention in luminescence-based bioanalysis due to their abundant optical and tunable surface physicochemical properties. However, luminescent nanomaterials often suffer from serious autofluorescence and light scattering interference when applied to complex biological samples. Time-resolved luminescence methodology can efficiently eliminate autofluorescence and light scattering interference by collecting the luminescence signal of a long-lived probe after the background signals decays completely. Lanthanides have a unique $[Xe]4f^N$ electronic configuration and ladder-like energy states, which endow lanthanide-doped nanoparticles with many desirable optical properties, such as long luminescence lifetimes, large Stokes/anti-Stokes shifts, and sharp emission bands. Due to their long luminescence lifetimes, lanthanide-doped nanoparticles are widely used for high-sensitive biosensing and high-contrast bioimaging via time-resolved luminescence methodology. In this review, recent progress in the development of lanthanide-doped nanoparticles and their application in time-resolved biosensing and bioimaging are summarized. At the end of this review, the current challenges and perspectives of lanthanide-doped nanoparticles for time-resolved bioapplications are discussed.

1. Introduction

Due to the quantum size effect, luminescent nanomaterials show unique properties that are different from their bulk counterparts,[1,2] such as blue shift of absorption bands,[3,4] size-dependent luminescence,[5–7] localized surface plasmon resonance,[8,9] and significantly enhanced energy transfer efficiency.[10] In addition, with the rapid development of synthetic methodology, luminescent nanomaterials with tunable shape and size can be obtained, and their luminescent properties can be readily tailored by adjusting the chemical composition, crystal structure, morphology, and size.[6,11,12] During the past few decades, a great variety of luminescent nanomaterials has been fabricated, including inorganic quantum dots,[13,14] upconversion nanoparticles,[15,16] persistent luminescence nanoparticles,[17,18] organic polymers,[19,20] and perovskite nanomaterials.[21–25] These luminescent nanomaterials are widely applied in bioanalysis, disease diagnosis, display, and catalysis.[26–29] Since nanomaterials can be tailored to accommodate biomolecules in size, the luminescent properties of nanoparticles can be significantly changed upon binding to biomolecules.[30,31] Moreover, nanoparticles can effectively accumulate at a tumor site through the enhanced permeability and retention effect, making them suitable for tumor diagnosis and therapy.[32,33] Nevertheless, there are still some challenges to be addressed in the biomedical applications of luminescent nanomaterials, primarily the autofluorescence and light scattering interference.[34,35] These background signals can seriously attenuate the probe signals, resulting in significantly decreased detection sensitivity and imaging resolution.[34,36,37] Therefore, the development of luminescent nanomaterials capable of eliminating autofluorescence and light scattering interference is of great significance for the application of luminescent nanomaterials in the life sciences.

Time-resolved method has been widely used in fluorescence analysis to eliminate autofluorescence and light scattering interference.[38–42] For time-resolved luminescence analysis, long-lived luminescent probes are required. Since the lifetime of autofluorescence or scattered light is short compared to that of a long-lived luminescent probe, the luminescence signal of long-lived probes can be collected after the background signals decay completely, effectively eliminating autofluorescence and light scattering interference.[39,42] Therefore, the detection sensitivity and imaging resolution of fluorescence analysis can be significantly improved by time-resolved luminescence methodology. In the past decades, time-resolved luminescence methods have attracted much attention. Huang co-workers designed a series of iridium complexes for background-free monitoring of hypoxia in living cells.[43–45] Chen's group designed a variety of lanthanide-doped nanomaterials and used them as long-lived probes to achieve high sensitivity detection of biotin and alpha-fetoprotein.[46–49]

Q. Q. Ma, Dr. J. Wang, Z. H. Li, X. B. Lv, Prof. Q. Yuan
Key Laboratory of Analytical Chemistry for Biology and Medicine
(Ministry of Education)
College of Chemistry and Molecular Sciences
Wuhan University
Wuhan 430072, China
E-mail: yuanquan@whu.edu.cn
L. Liang
Molecular Science and Biomedicine Laboratory
Institute of Chemical Biology and Nanomedicine
State Key Laboratory of Chemo/Biosensing and Chemometrics
College of Chemistry and Chemical Engineering
Hunan University
Changsha 410082, China

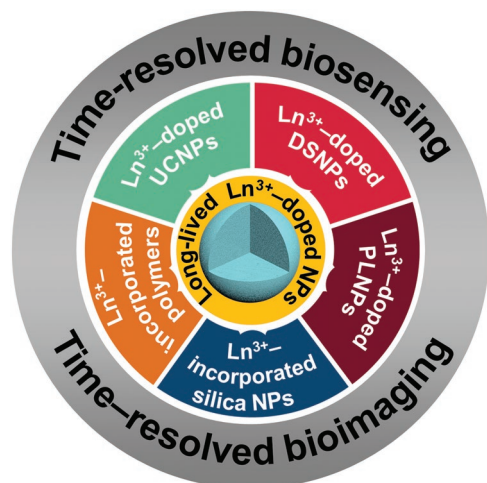The ORCID identification number(s) for the author(s) of this article can be found under https://doi.org/10.1002/smll.201804969.

Figure 1. Illustration of different kinds of lanthanide-doped nanoparticles for time-resolved biosensing and bioimaging applications.

Qinqin Ma received her B.S. from the College of Chemistry and Molecular Sciences, Wuhan University in 2015. She is currently pursuing her Ph.D. degree under the supervision of Prof. Quan Yuan at the Key Laboratory of Analytical Chemistry for Biology and Medicine (Ministry of Education), College of Chemistry and Molecular Sciences, Wuhan University. Her current research focuses on controlled synthesis of novel luminescent nanomaterials for biomedical applications.

Jie Wang received his B.S. from the School of Chemical Engineering and Pharmacy, Wuhan Institute of Technology in 2012. He obtained his Ph.D. degree in analytical chemistry under the supervision of Prof. Quan Yuan at the Key Laboratory of Analytical Chemistry for Biology and Medicine (Ministry of Education), College of Chemistry and Molecular Sciences, Wuhan University. He is now performing postdoctoral research work with Professor Quan Yuan at Wuhan University. His current research interests include the development of functional nanomaterials for biosensing and bioimaging.

Quan Yuan is currently a full professor in the College of Chemistry and Molecular Sciences at Wuhan University. She received her B.S. from College of Chemistry and Molecular Sciences, Wuhan University in 2004. She obtained her Ph.D. from the College of Chemistry and Molecular Engineering, Peking University in 2009. She then performed post-doctoral research with Prof. Weihong Tan at the University of Florida from 2009 to 2012. In 2012, she joined the Key Laboratory of Analytical Chemistry for Biology and Medicine (Ministry of Education), Wuhan University. Her research interests include controlled synthesis of functional nanomaterials and their biomedical applications.
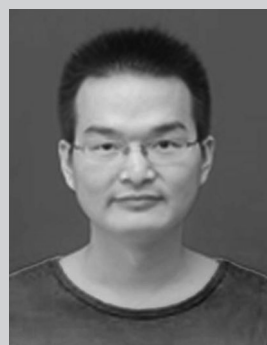
The discovery of long-lived luminescent nanomaterials is very important for promoting the development of time-resolved luminescence methodology. The lanthanides (Ln^{3+}) have unique $[Xe]4f^N$ electronic configurations and ladder-like energy states, making them excellent luminescent centers.[50–52] When doped into nanomaterials, lanthanides endow the materials with unique luminescent properties including long luminescence lifetimes, multiple emission bands, narrow emission bandwidths, and large Stokes/anti-Stokes shifts.[50,52] The luminescence of lanthanide-doped nanomaterials originates from the intraconfigurational 4f–4f transitions of lanthanides, and the Laporte-forbidden f–f transitions endows them with long luminescence lifetimes[44,50,53] (usually in the microsecond to millisecond range, which is significantly longer than that of fluorescent biomolecules). Therefore, lanthanide-doped nanomaterials are ideal candidates for time-resolved fluorescence analysis as long-lived probes. In the past decades, lanthanide-doped nanomaterials have been widely used in time-resolved biosensing and bioimaging.[40] In this review, we summarize recent process in the design and applications of long-lived lanthanide-doped nanomaterials in time-resolved luminescent biosensing and bioimaging (**Figure 1**). First, we provide a brief overview of the time-gated luminescence technique and the optical properties of Ln^{3+}-doped nanomaterials. Second, we summarize the utilization of long-lived nanomaterials, including lanthanide-doped upconversion nanoparticles, lanthanide-doped downshifting nanoparticles, lanthanide-doped persistent luminescence nanoparticles, lanthanide-incorporated organic polymers, and lanthanide-incorporated silica nanoparticles, for autofluorescence-free biosensing and bioimaging. Finally, we consider the future prospects and challenges of time-resolved biosensing and bioimaging based on lanthanide-doped nanoparticles.

2. Time-Gated Luminescence (TGL) Technique

TGL technique operates within the time-domain and aims at detection of events that occur at microsecond to millisecond timescales.[54] It has been demonstrated to be an ideal method to eliminate autofluorescence and light scattering interference. The TGL system usually consists of a pulsed excitation source to excite the long-lived probe, a rotating mechanical chopper to

ADVANCED
SCIENCE NEWS
www.advancedsciencenews.com

NANO · MICRO
small
www.small-journal.com

Figure 2. Mechanism of autofluorescence elimination based on time-gated luminescence technique. Reproduced with permission.[49] Copyright 2011, John Wiley and Sons.

Figure 3. The energy-level diagrams of Ln[3+] ions. Reproduced with permission.[59] Copyright 2015, Royal Society of Chemistry.

block the excitation and short-lived fluorescence signals, and a detector to collect the long-lived signal from the probe.[54–56] The selection of pulsed excitation sources and the rotation rate of the chopper depend on the lifetime and excitation wavelength of the probe. In a typical TGL measurement (**Figure 2**),[49] the long-lived luminescence signal of the probe is collected by synchronizing the chopper rotation speed with the pulse frequency. During the interval between two consecutive pulses within the pulses train, the short-lived signals and long-lived luminescence signal decay. After the short-lived background signal decays beyond the detection limit of the detector, the chopper turns open to leave light passing through it and the long-lived luminescence signal of the probe is collected. In this way, the excitation and short-lived background signal is blocked. Because the luminescence intensity of the long-lived probe decreases rapidly with time, the collected signal is usually very weak. Thus, repeated measurements are needed to enhance the detection accuracy and sensitivity. With the TGL technique based on the time-resolved principle, the deleterious short-lived background noise is eliminated and remarkably enhanced signal-to-noise ratio can be obtained. Thereby high detection sensitivity is achieved compared to conventional steady-state fluorescence analysis.

3. Long Luminescence Lifetimes of Lanthanide-Doped Nanomaterials

The lanthanides comprise the fifteen consecutive elements ranging from lanthanum to lutetium, which located at the sixth period and IIIB group in the Periodic Table. When doped into nanomaterials, lanthanides are usually in the stable trivalent state, Ln[3+], with similar electronic configurations ([Xe]4f[N]) with unfilled electron shell structure $4f^N$ ($N = 1$–14).[50,57,58] The electronic configurations generate a rich variety of electronic levels (**Figure 3**), resulting in unique optical properties.[59] Lanthanide ions exhibit three types of electronic transitions: the Laporte-forbidden intraconfiguration f–f transitions, 4f–5d transitions and charge-transfer transitions,[60] in which the forbidden intra-configuration f–f transitions are the most common. Since the 4f electrons are efficiently shielded by the outer filled $5s^2 5p^6$ electron subshells, the 4f energies are well defined and relatively insensitive to the chemical environments, including the

crystal-field (CF) environment.[50,59] The emission wavelengths of lanthanide ions cover the entire spectrum from UV to near-infrared (NIR) region because of their multiple electronic levels. The emissions are usually sharp and rather pure. Moreover, since the intraconfiguration f–f transitions are principle-forbidden, the lifetimes of the excited states are considerably long, usually in the microsecond to millisecond range.

Due to these unique optical properties, a variety of lanthanide-doped nanomaterials have been developed, including lanthanide-doped upconversion nanocrystals, lanthanide-doped downshifting nanoparticles, lanthanide-doped persistent luminescence nanoparticles, lanthanide-incorporated organic polymers, and lanthanide-incorporated silica nanoparticles. Lanthanide doping endows these nanomaterials with unique luminescence properties, including long luminescence lifetimes, sharp emission bands, large Stokes/anti-Stokes shifts, and tunable excitation and emission wavelengths. The long luminescence lifetimes make lanthanide-doped nanomaterials ideal long-lived probes to eliminate autofluorescence and light scattering interference via time-resolved luminescence methodology.[40] The lanthanide-doped nanomaterials have been widely studied for time-resolved biosensing and bioimaging with high sensitivity and resolution.

4. Lanthanide-Doped Upconversion Nanoparticles for Time-Resolved Biosensing and Bioimaging

Lanthanide-doped upconversion nanoparticles (Ln[3+]-doped UCNPs) can absorb two or more low energy photons and generate a single high-energy photon through a nonlinear optical process.[59,61,62] The doped lanthanides with abundant energy levels endow Ln[3+]-doped UCNPs with many energy transfer pathways for UC emissions, including excited state absorption, energy transfer upconversion, photon avalanche, cooperative energy transfer, and energy migration-mediated upconversion.[53,59] Because a near-infrared (NIR) laser is used as the excitation source, deep tissue penetration is possible due to reduced absorption and light scattering by biological tissues. In addition, Ln[3+]-doped UCNPs exhibit long luminescence lifetime on the order of microseconds, thus enabling use of TGL to

ADVANCED
SCIENCE NEWS
www.advancedsciencenews.com

NANO · MICRO
small
www.small-journal.com

eliminate the short-lived autofluorescence and scattered light. These properties make Ln^{3+}-doped UCNPs the next generation of nanomaterials for bioapplications.

4.1. Strategies for Tuning the Upconversion Luminescence Lifetime

It is significant to adjust the luminescence lifetimes of UCNPs for time-resolved analysis. On the one hand, long luminescence lifetimes can enable reduction of autofluorescence and light scattering interference, while still maintaining a strong luminescence signal for improved sensitivity of detection. On the other hand, in the life sciences, simultaneous identification of multiple distinctive species is commonly required to avoid false positive results and improve the reliability of biodetection.[63,64] Adjusting the luminescence lifetimes of UCNPs can lead to additional distinguishable dimensions for simultaneous detection of multiple species. Several strategies have been reported to tune the lifetimes of Ln^{3+}-doped UCNPs, such as varied concentrations of sensitizer and activator,[63] epitaxial growth of passivated shells[65] and core–shell structure-mediated energy migration.[64,66–69]

Changing the concentrations of sensitizer and activator has been demonstrated to be a good way to regulate the luminescence lifetimes of UCNPs. In 2014, Jin et al. developed an approach to precisely tune the luminescence lifetimes of lanthanide-doped nanocrystals by doping sensitizer Yb^{3+} ions and activator Tm^{3+} ions at varied concentrations into $NaYF_4$ nanocrystals.[63] In their lifetime multiplexing concept (**Figure 4**a), adjusting the doping concentration of Tm^{3+} can lead to varying sensitizer-emitter distances, and energy transfer from sensitizers to activators at varied distances can achieve lifetime tunability. In that work, $NaYF_4$:Yb,Tm nanocrystals with concentrations of Tm^{3+} in the range of 0.2–4% and Yb^{3+} fixed at 20% were prepared. The resulting luminescence lifetimes observed in the blue emission band of Tm^{3+} varied from 48 to 668 µs when the concentration of Tm^{3+} was reduced from 4% to 0.2% (Figure 4b), showing that the lifetimes of rare-earth doped nanocrystals can be easily tuned by simply adjusting the doping concentration of sensitizer and activator. Since the lifetimes of nanocrystals are about three orders of magnitude longer than that of autofluorescence, the long-lived nanoparticles are suitable for autofluorescence-free bioapplications through time-resolved measurements. Furthermore, this lifetime multiplexing strategy can lead to a variety of nanocrystals with distinguishable lifetimes, thus providing a powerful approach to cope with the detection of multiple species.

The core–shell structure designation is another efficient method to endow nanoparticles with prolonged luminescence lifetimes, enhanced luminescence intensity, and multiple excitation and emission wavelengths. Yan and co-workers have reported the construction of core–shell UCNPs to realize enhanced upconversion emission intensity and prolonged luminescence lifetime.[65] In this study, the β-$NaGdF_4$:Yb,Er@CaF_2 core–shell nanoparticles were obtained through a cation exchange-launched heteroepitaxy method. Due to cation exchange between Ca^{2+} and Na^+, a hexagonal-to-cubic transition layer was formed on the surface of β-NaLnF$_4$

nanoparticles, which could remediate the dissimilar structure between β-$NaLnF_4$ and CaF_2. The hexagonal-to-cubic transition layer further enabled the heteroepitaxial growth of a CaF_2 shell. The emission intensity of the obtained core–shell nanoparticles at 542 nm was enhanced by 55.5 times and the emission lifetime was prolonged from 89 to 162 µs. The CaF_2 shell can separate luminescent Er^{3+} from surface defects and ligand vibrations quenching, as well as suppress the interfacial diffusion of Ln^{3+}, leading to enhanced emission and prolonged lifetime.

Yan and co-workers further developed a core–shell structure approach to simultaneously realize emission color and lifetime multiplexing in single UCNPs.[67] In their design, the nanoparticles consisted of two noninterfering regions separated by an optically inert layer (Figure 4c). In the $NaGdF_4$:Yb,Tm@$NaGdF_4$:Tb@$NaYF_4$@$NaYF_4$:Yb,Er@$NaYbF_4$:Nd@$NaYF_4$ nanoparticles, Yb^{3+}/Tm^{3+}/Tb^{3+} were doped into the inner region, and Yb^{3+}/ Er^{3+}/Nd^{3+} were incorporated into the outer region separated with an inert $NaYF_4$ layer. The approach endowed the nanoparticles with different colors and luminescence lifetimes under different excitations. The inner region can be excited with a 980 nm laser, and the outer region can respond to both 980 and 808 nm excitations. With such an elegant structure design, the blue emission of Tm^{3+} was obtained with 980 nm laser excitation and green emission of Er^{3+} was triggered by stimulation with 808/980 nm lasers. Furthermore, with incorporation of Tb^{3+} in the inner region, sequential energy migration from Tm^{3+} to Tb^{3+} allowed long Tb^{3+} lifetime in the milliseconds range (Figure 4d). This strategy achieves effective control of emission color and lifetime in UCNPs, and will greatly expand the application of luminescent nanomaterials for optical multiplexing.

Liu et al. also developed a method to adjust the luminescence lifetimes of UCNPs by mediating energy migration from a short-lived emitter to a long-lived emitter embedded in the core–shell structure.[68] In $NaGdF_4$:Mn@$NaGdF_4$:Yb/Tm@$NaYF_4$ nanoparticles, Mn^{2+} doped $NaGdF_4$ served as the core, Yb/Tm-doped $NaGdF_4$ was used as the first shell layer and pure $NaYF_4$ were further coated as the passivating layer (Figure 4e). The $NaGdF4$:Yb/Tm shell was activated with 808/980 nm excitation, and the absorbed energy was transferred to long-lived Mn^{2+} through a $Yb^{3+}{\rightarrow}Tm^{3+}{\rightarrow}Gd^{3+}{\rightarrow}Mn^{2+}$ pathway. The Gd^{3+} serve as the energy migrators to enable Mn^{2+} emission by an energy migrant upconversion process. In this way, long-lived Mn^{2+} doped upconversion nanoparticles were fabricated. The resulting core–shell–shell nanoparticles showed characteristic emission bands of Tm^{3+} and a broad emission of Mn^{2+} in the region of 490–625 nm. The lifetime of Mn^{2+} emission at 550 nm was 39 ms, which was much longer than that of Tm^{3+} emission centered at 475 nm (0.6 ms) (Figure 4f). The multilayer structure-based energy migrant strategy can be used to design other kinds of UCNPs with long-lived upconversion luminescence, further contributing to in vivo bioapplications, as well as data storage and security applications.

4.2. Lanthanide-Doped Upconversion Nanoparticles for Time-Resolved Biosensing

Since the luminescence lifetime of UCNPs is independent of concentration and excitation power, a variation in lifetime can
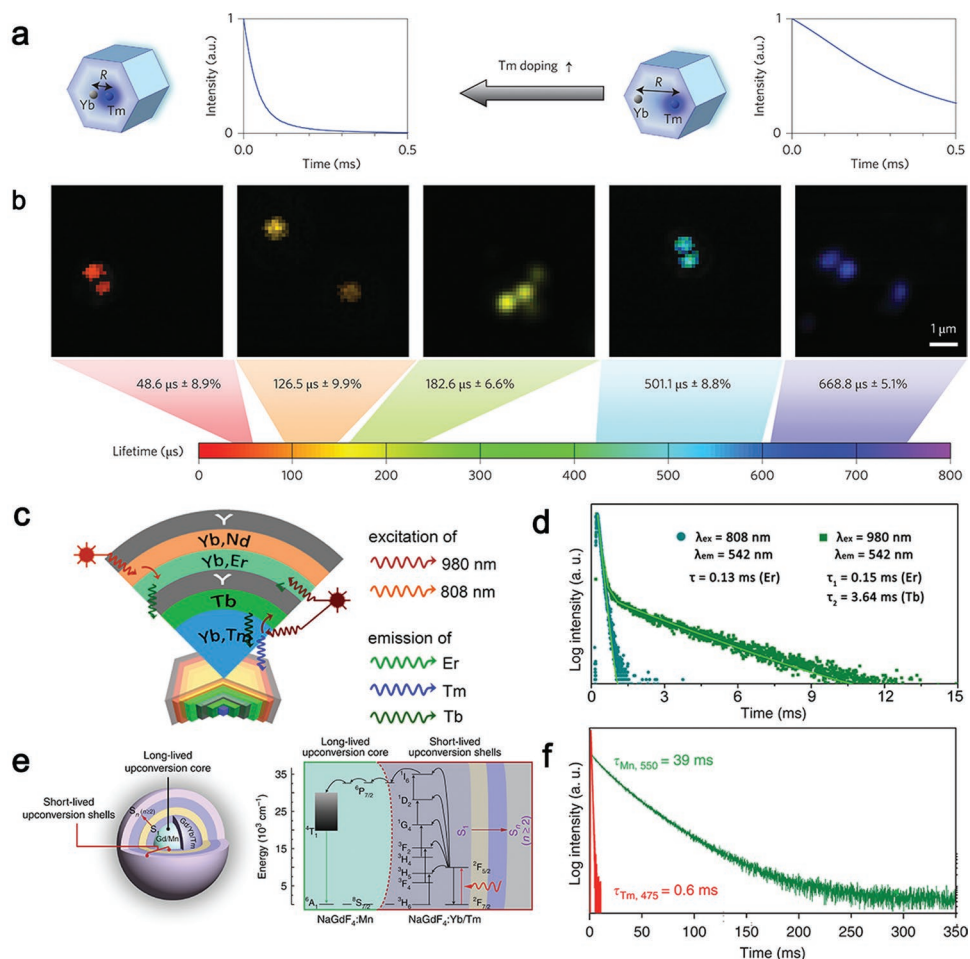
Figure 4. a) Scheme of lifetime tuning strategy. b) Time-resolved confocal images of NaYF$_4$:Yb,Tm nanocrystals doped with different concentrations of Tm^{3+}. a,b) Reproduced with permission.[63] Copyright 2013, Springer Nature. c) Schematic illustration of multicompartment core/shell upconversion nanoparticles with spectral and lifetime multiplexing. d) Decay curves of the multicompartment core/shell upconversion nanoparticles under 808 and 980 nm excitation. c,d) Reproduced with permission.[67] Copyright 2017, American Chemical Society. e) Structure and energy transfer pathway of multilayer upconversion nanoparticles with long-lived Mn^{2+} luminescence. f) Luminescence decay curves of multilayer upconversion nanoparticles under excitation at 980 nm. e,f) Reproduced with permission.[68] Copyright 2017, Springer Nature.

indicate interactions with surroundings. Furthermore, due to the multiple and sharp emission bands, UCNPs can be employed for simultaneous detection of multiple substances. Detection accuracy can be improved by using UCNPs as ratiometric fluorescent probes. Many substances, varying from inorganic ions to cells, have been detected with lanthanide-doped UCNPs.[70–73] Biosensing with UCNPs as labels is commonly based on the direct detection of upconversion luminescence or the luminescence resonance energy transfer signal.

As mentioned above, Jin and co-workers prepared a series of NaYF$_4$:Yb(20%),Tm(x%) nanoparticles with lifetimes ranging from 48 to 668 µs by adjusting the doped concentration of Tm^{3+}. They further used NaYF$_4$:Yb(20%),Tm(1%) with lifetime of 160 µs and NaYF$_4$:Yb(20%),Tm(4%) with lifetime of 40 µs to detect single *Giardia lamblia*, a parasite that causes the diarrheal disease known as giardiasis, with time-gated orthogonal scanning automated microscopy platform.[63] An antibody of *Giardia lamblia* was functionalized on the surface of UCNPs and the antibody-functionalized nanoparticles were used to detect *Giardia lamblia*

by targeted binding with the surface antigen (**Figure 5**a). The *Giardia lamblia* cysts were successfully labeled with antibody-functionalized NaYF$_4$:Yb(20%),Tm(1%) and NaYF$_4$:Yb(20%),Tm(4%) (Figure 5b). Moreover, the UCNPs stained *Giardia lamblia* images showed no photobleaching over 4 h of continuous illumination. These results indicate that NaYF$_4$:Yb(20%),Tm(x%) nanoparticles can serve as robust labeling materials for biodetection.

Recently, Zhang and co-workers prepared many kinds of NaGdF$_4$:Yb, Ln^{3+}@NaYF$_4$:Yb@NaNdF$_4$:Yb@NaYF$_4$ nanoparticles having a core–shell–shell structure with Yb^{3+}/Ln^{3+}-doped activation core, Yb^{3+}-doped energy relay layer, Nd^{3+}/ Yb^{3+}-doped energy absorbance layer and inert outer layer.[64] The doped Ln^{3+} in the activation core endowed the prepared UCNPs with multiple luminescence emission colors and decay lifetimes under illumination with an 808 nm laser. These nanoparticles were incorporated into porous polystyrene microspheres and the composites were further used for simultaneous detection of human papilloma virus (HPV) subtypes in patient samples by using a time-resolved imaging scanning system.
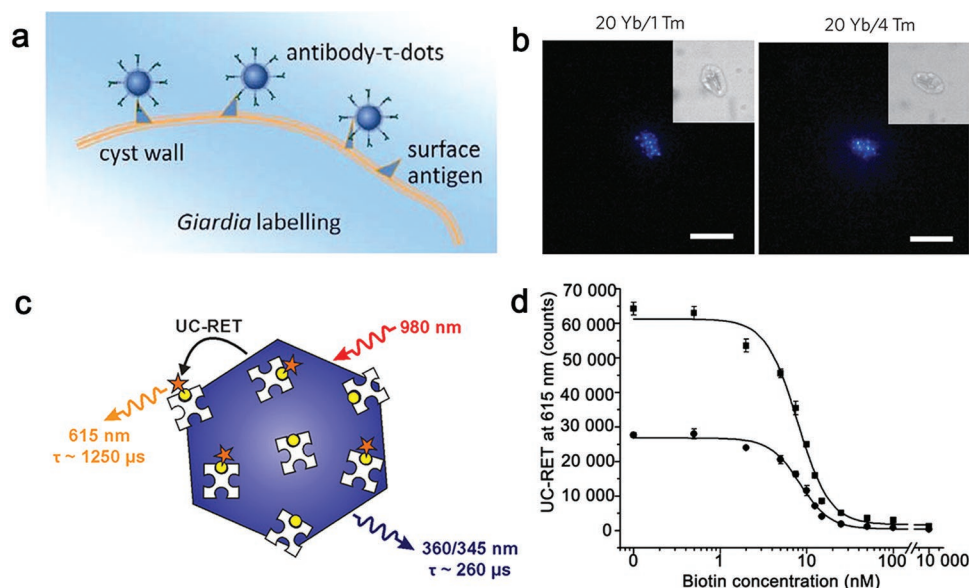
Figure 5. a) Scheme of cellular uptake of antibody-functionalized NaYF$_4$:Yb,Tm. b) Time-resolved confocal images of NaYF$_4$:Yb,Tm nanoparticles labeled with Giardia cysts. a,b) Reproduced with permission.[63] Copyright 2013, Springer Nature. c) Principle of upconversion resonance energy transfer for biotin detection with 980 nm excitation. d) Standard curves of biotin detection with temporal resolution mode (circles) or steady-state (squares). c,d) Reproduced with permission.[74] Copyright 2016, American Chemical Society.

Lahtinen et al. designed an upconversion resonance energy transfer method for biotin detection.[74] In their design (Figure 5c), NaKYF$_4$:Yb,Tm UCNPs with characteristic Tm^{3+} emission at 365 nm (260 µs) were used as donors and long-lived europium(III) complex (emission at 615 nm, 1250 µs) was used as the acceptor. The UCNPs were first conjugated with streptavidin, and further bonded to a biotin-labeled europium(III) complex to construct the upconversion resonance energy transfer system. In this system, energy could transfer from UCNPs to Eu(III) complex upon 980 nm excitation, leading to the occurrence of sensitized emission of the Eu(III) complex with long lifetime. This enabled temporal measurement of Eu(III) complex emission after the UCNPs emission completely decayed. Because of its strong binding affinity to the avidin-functionalized UCNPs, free biotin can compete with the biotinylated Eu(III) complex to bind to the UCNPs. Therefore, the emission intensity of the europium(III) complex at 615 nm is reduced with increasing concentrations of biotin. Through this approach, biotin in a wide range of concentrations was detected and a low limit of detection (3.0×10^{-9} M) was obtained (Figure 5d).

4.3. Lanthanide-Doped Upconversion Nanoparticles for Time-Resolved In Vivo Bioimaging

During the past few years, lanthanide-doped upconversion nanoparticles have been demonstrated to be ideal probes for in vivo imaging.[52,53,75] Lanthanide-doped upconversion nanoparticles with a wide range of compositions, sizes and shapes can be easily obtained with the development of synthetic methodology to provide tunable luminescence lifetimes. Besides, UCNPs can be functionalized with a variety of recognition molecule, such as antibodies and aptamers, for targeted bioimaging. As mentioned above, a low-power NIR continuous-wavelength (CW) laser at 808 or 980 nm can be used as the excitation source for reduced light scattering and autofluorescence. However, some biomolecules, for example melanin, can be excited under NIR light illumination, so the autofluorescence still presents in the NIR range. To further eliminate the autofluorescence interference, the long luminescence lifetime property of UCNPs has been employed in bioimaging by combining with time-gated luminescence technique.

In 2016, Jin and co-workers developed a time-gated imaging system to realize high-contrast time-gated imaging of mice with long-lived UCNPs probes.[76] The time-gated imaging system contained a pulsed 980 nm laser, a camera lens, an optical chopper, a microscope eyepiece, and an EMCCD camera (**Figure 6**a). Time-gated imaging was realized by synchronizing the chopper with the pulsed laser to open the detection path during the interval between two consecutive pulses when the short-lived interfering signals had decayed. In their work, hydrophilic NaLuF$_4$:Yb,Tm UCNPs that are excited at 980 nm and emit at 800 nm, were used as the long-lived probe, and a pulsed laser was used to reduce the overall thermal accumulation to the mice as compared to the continuous-wave laser (Figure 6b). Although the temperature of the mice increased over 25 °C in 30 s under the CW laser illumination, the temperature changed negligibly under pulsed laser irradiation. The UCNPs were subcutaneously injected into the Kunming mice, which were further subjected to the designed time-gated imaging. The resulting time-gated image was clear without any autofluorescence or scattered light interference, while the non-time-gated image showed a stronger background signal (Figure 6c), demonstrating that UCNPs have good potential for background-free NIR imaging with a time-gated imaging system.
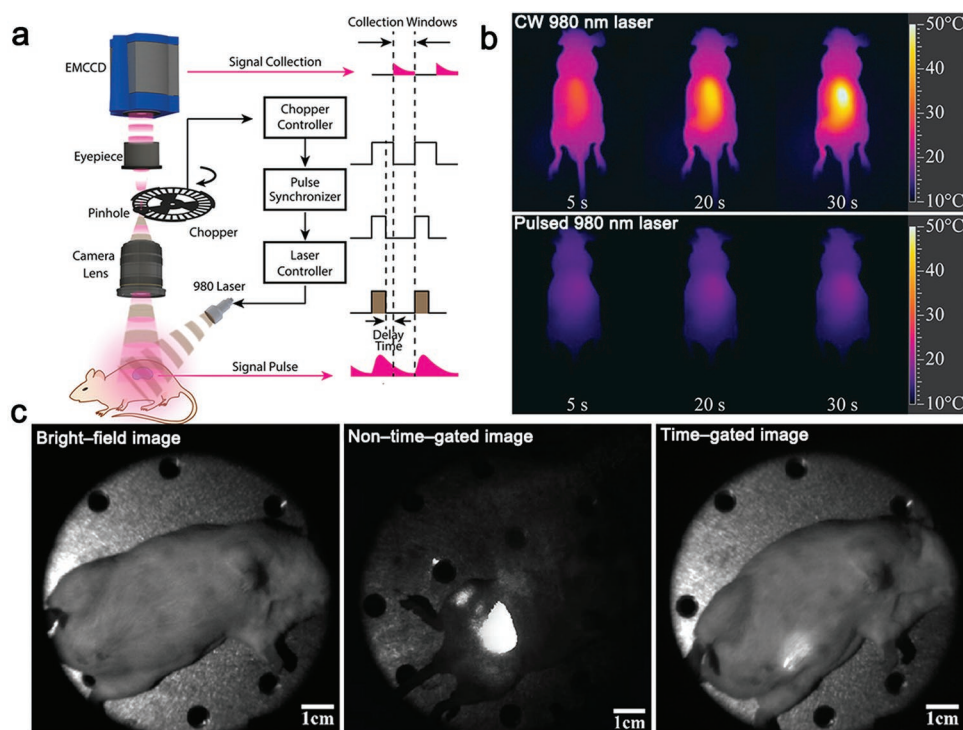
ADVANCED
SCIENCE NEWS

www.advancedsciencenews.com

NANO · MICRO
small

www.small-journal.com

Figure 6. a) Schematic diagram of the time-gated imaging system. b) Thermal images of Kunming mouse illuminated with CW 980 nm laser (above) and pulsed 980 nm laser (below) for 5 s, 20 s, and 30 s. c) Bright-field image (left), non-time-gated image (middle), time-gated image (right) of NaLuF$_4$:Yb,Tm UCNPs treated Kunming mouse under a white LED and 980 nm excitation illumination. All panels reproduced with permission.[76] Copyright 2016, American Chemical Society.

5. Lanthanide-Doped Downshifting Nanoparticles for Time-Resolved Biosensing and Bioimaging

Compared with UCNPs, downshifting nanoparticles (DSNPs) are more common luminescent nanomaterials. DSNPs absorb high energy photons and then emit low energy photons.[77–79] Generally, lanthanide-doped downshifting nanoparticles also exhibit desirable properties, such as long luminescence lifetimes, multiple emission bands, narrow emission bandwidths, and large Stokes shifts. In addition, lanthanide-doped DSNPs can be activated by light in the UV to NIR range, and they usually exhibit much higher quantum yields than UCNPs. Moreover, NIR-to-NIR lanthanide-doped DSNPs have been prepared and the emission of these DSNPs can be tuned in the second near-infrared (NIR-II) window, which offers enhanced tissues penetration and much lower light scattering.[77,80] Due to these excellent properties, lanthanide-doped DSNPs have been widely used in biosensing, monitoring the biological processes, and imaging-guided therapy.

5.1. Strategies for Tuning the Downshifting Luminescence Lifetime

As described above, the long luminescence lifetimes make luminescent nanomaterials highly efficient in the elimination of autofluorescence and light scattering interference via time-resolved luminescence methodology. In addition, luminescent nanomaterials with tunable luminescence lifetimes can be employed for

simultaneous detection of multiple substances. Probes with different colors are frequently used to achieve simultaneous quantitative detection of different analytes. However, spectral overlap of the probes is a serious problem that impedes their biosensing application. Developing probes with tunable luminescence lifetimes can be another coding dimension for achieving quantitative multiplexing. Some strategies have been developed to tune the lifetimes of lanthanide-doped DSNPs, including varying the concentration of luminescent centers, energy transfer control with core–shell structure and hetero-valence ion doping.[80,81]

Recently, Zhang and co-workers have made advances in tuning the lifetimes of lanthanide-doped DSNPs.[80] The DSNPs with core–multishell structure were designed in the form of NaGdF$_4$@NaGdF$_4$:Yb,Er@NaYF$_4$:Yb@NaNdF$_4$:Yb (**Figure 7**a). In the core–multishell structure, the Nd^{3+} doped in the outer layer absorbed 808 nm excitation photons, and then transferred the energy to Yb^{3+} doped in the same layer. The energy was then relayed within the Yb^{3+} sublattice and eventually transferred to Er^{3+} emitters doped in the inner layer to generate downshifting luminescence at 1525 nm. The NaGdF$_4$ insert core was included to enable uniform epitaxial growth of multiple shells, in order to prepare a series of core–multishell nanoparticles with a small size of about 20 nm (Figure 7b). Based on this design, two approaches for adjusting luminescence lifetimes were proposed. First, extending the energy transfer process by increasing the thickness of energy relay layer could prolong luminescence lifetime. Second, accelerating the conversion of absorbed energy into emission by increasing the Er^{3+} concentration could shorten luminescence lifetime. With the first

strategy, the luminescence lifetime at 1525 nm was tuned from 1.25 ms to 20.9 ms by increasing the thickness of energy relay layer from 0 to 7 nm (Figure 7c). With the second strategy, the luminescence lifetime was adjusted from 2.75 ms to 292 μs by varying the Er^{3+} concentration from 2% to 30% (energy relay shell thickness, 0.9 nm) (Figure 7d). Altogether, nanoparticles with a wide range of luminescence lifetimes from several μs to tens of milliseconds were obtained through the above two approaches (Figure 7e). The properties of tunable lifetime and NIR-to-NIR emission make core–multishell nanoparticles promising in high-sensitive biosensing and high-contrast bioimaging.

Hetero-valence ion doping is an efficient way to tune the optical properties of luminescent nanomaterials. Chen and co-workers developed a strategy to synthesize ultrasmall CaF_2:Ce,Tb DSNPs based on Na^+ doping.[81] The prepared Na^+-doped DSNPs have high crystallinity, enhanced luminescence intensity, and prolonged lifetime. The luminescence intensity of doped nanoparticles synthesized with Na^+ was 34 times higher than that of undoped nanoparticles. The luminescence lifetime was prolonged from 1.25 ms to about 12.0 ms by increasing the concentration of Na^+ from 0×10^{-3} to 2.5×10^{-3} M. The enhanced luminescence intensity and prolonged lifetime were attributed to the doped Na^+, which could modify the crystal-field environment of the emitters and reduce the quenching of Tb^{3+} by charge compensation. Nanoparticles with such high luminescence intensity and long luminescence lifetime are favorable for biosensing and bioimaging.

5.2. Lanthanide-Doped Downshifting Nanoparticles for Time-Resolved Biosensing

Lanthanide-doped DSNPs have emerged as alternative bio-probes to conventional fluorescent probes. They have attracted much attention because of their superior features including long luminescence lifetimes, multiple emission bands, large Stokes shifts, and high photostability.[40] Long luminescence
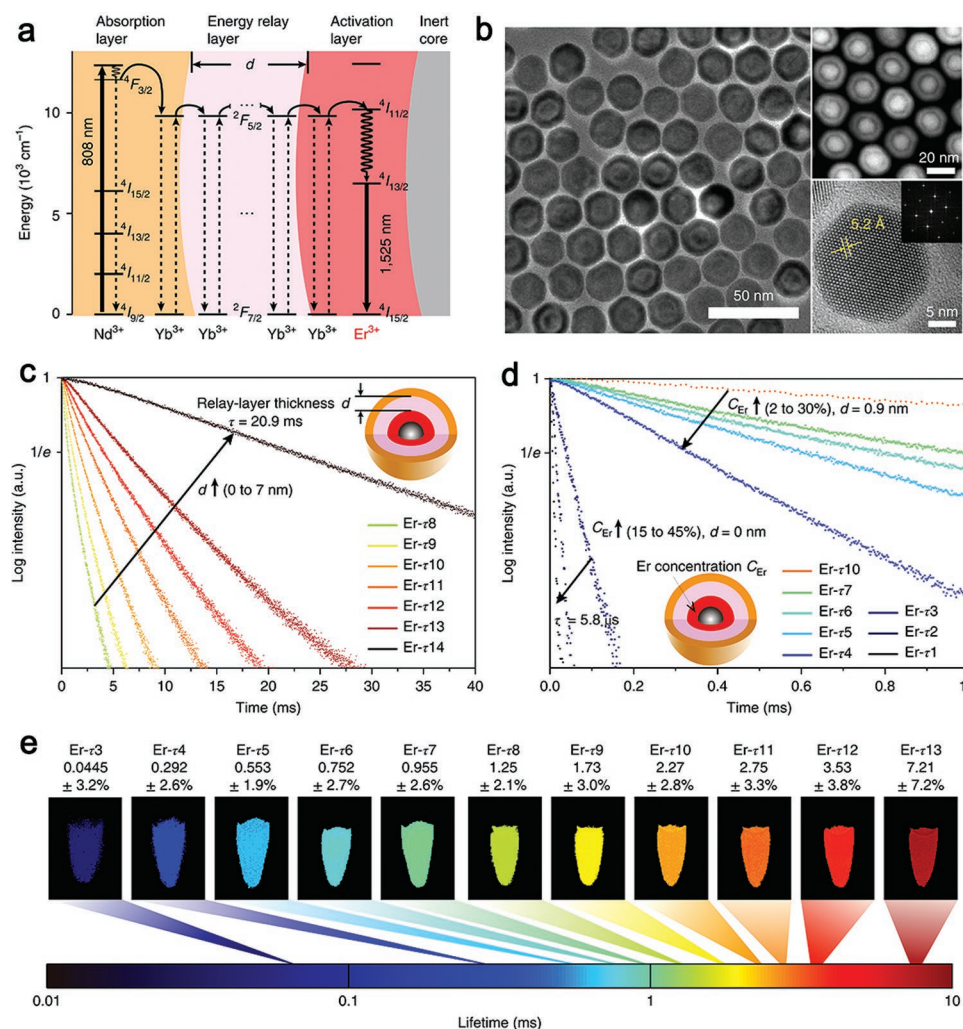
Figure 7. a) Schematic representation of energy transfer in core–multishell nanoparticles. b) TEM, HAADF-STEM, and HRTEM images of core–multi-shell nanoparticles. c) Luminescence decay curves of nanoparticles with increased thickness of energy relay layer. d) Luminescence decay curves of nanoparticles with increased Er^{3+} doping concentration (energy relay shell thickness, 0 or 0.9 nm). e) Lifetime images of core–multishell nanoparticles obtained by time-resolved imaging system. All panels reproduced with permission.[80] Copyright 2018, Springer Nature.

ADVANCED
SCIENCE NEWS
www.advancedsciencenews.com

NANO · MICRO
small
www.small-journal.com

lifetimes make lanthanide-doped DSNPs ideal probes for time-resolved biosensing without autofluorescence and light scattering interference. The multiple emission bands can enable DSNPs to be used as ratiometric luminescent probes to provide built-in correction for environment effects and achieve quantitative detection. Moreover, DSNPs with a variety colors and luminescence lifetimes can be easily prepared, enabling application for simultaneous detection of multiple substances. Due to these excellent properties, lanthanide-doped DSNPs have been widely investigated as bioprobes for highly sensitive biosensing.[46,48,49,82–85]

Time-resolved fluorescence immunoassay is one of the most sensitive bioassay techniques, due to the elimination of short-lived autofluorescence and light scattering from biological samples.[82] Chen's group has extensively studied time-resolved fluorescence immunoassay based on lanthanide-doped DSNPs. In 2013, they prepared sub-10 nm $CaF_2:Ln^{3+}$ DSNPs and used these nanoparticles for sensitive detection of avidin and uPAR through time-resolved fluorescence immunoassay.[81] Biotinylated $CaF_2:Ce,Tb$ (millisecond lifetime) was used as the probe for avidin detection via heterogeneous time-resolved fluorescence immunoassay (**Figure 8**a). The biotinylated $CaF_2:Ce,Tb$ was specifically bonded to avidin fixed on the wells and the unbounded nanoparticles were removed by washing. Quantitative detection of avidin was achieved by measuring the time-resolved luminescence (TRL) intensity of the NPs. The TRL intensity was gradually enhanced with increasing avidin

concentration (Figure 8b). This detection method showed linear response to avidin in the range of 0.3×10^{-9} to 10×10^{-9} M and a record low limit of detection (48×10^{-12} M) was reached. Also, the amino terminal fragment of urokinase plasminogen activator (ATF)-functionalized $CaF_2:Ce,Tb$ were employed as the probe for detecting a cancer biomarker, urokinase plasminogen activator receptor (uPAR), through time-resolved fluorescence resonance energy transfer (TR-FRET) assay (Figure 8c). Fluorescein isothiocyanate (FITC) showed a broad excitation band at 490 nm, which overlapped well with the emission of $CaF_2:Ce,Tb$. Therefore, the ATF-functionalized $CaF_2:Ce,Tb$ NPs acted as energy donors and FITC-labeled uPAR was used as energy acceptor in the TR-FRET assay. With the specific binding of ATF to uPAR, the excitation energy could be transferred from $CaF_2:Ce,Tb$ to FITC, leading to an increase of FITC lifetime. With increasing amounts of FITC-labeled uPAR, the emission of FITC at 520 nm was gradually enhanced and the emission of Tb^{3+} at 491 nm was decreased (Figure 8d). As a result, the concentration of uPAR was quantified by measuring the TR-FRET signal of FITC520/Tb491. The method showed linear response to uPAR in the range from 0.5 to 571×10^{-9} M and a limit of detection (LOD) of 328×10^{-12} M, which is comparable to the uPAR concentration in the serum of cancer patients. Moreover, they also used biotinylated $CaF_2:Ce,Tb$ to realize sensitive detection of avidin with a low LOD of 164×10^{-12} M based on the TR-FRET assay. In the past several years, they have prepared a large variety of long-lived DSNPs for biomolecule detection via
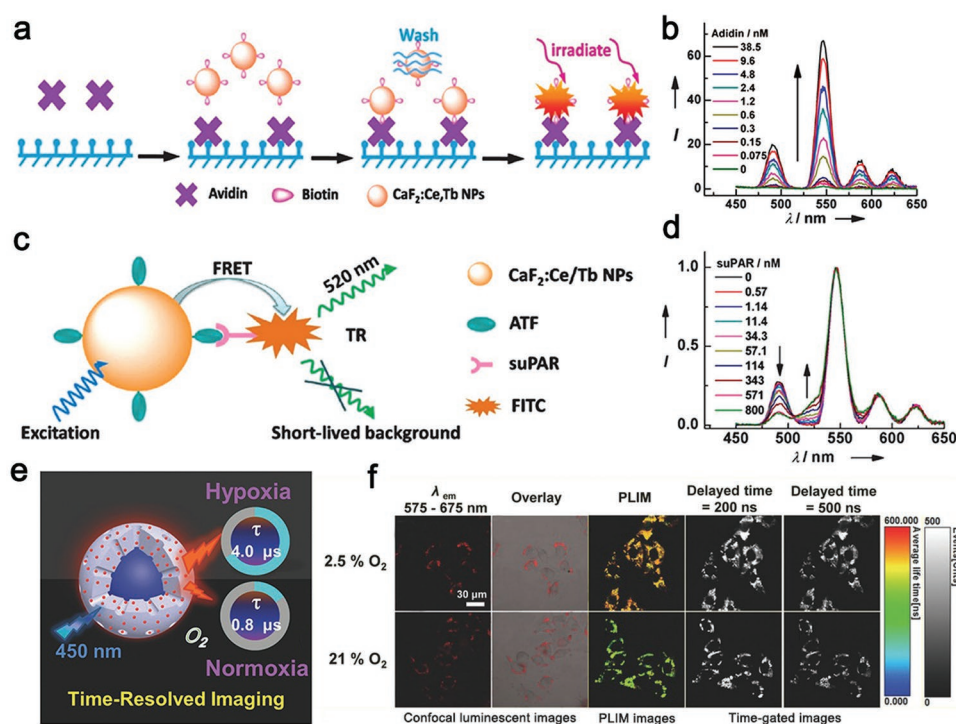

Figure 8. a) Scheme of the heterogeneous time-resolved fluorescence immunoassay for avidin detection. b) Time-resolved luminescence spectra of the bioassays in the presence of different concentrations of avidin. c) Schematic illustration of homogeneous TR-FRET assay for uPAR detection. d) TR-FRET spectra of the bioassay exposed to different concentrations of uPAR. a–d) Reproduced with permission.[81] Copyright 2013, John Wiley and Sons. e) Scheme of time-resolved detection of oxygen in living cells with UCNPs@mSiO2–Ir downshifting nanoparticles. f) Confocal luminescent images, PLIM images, and time-gated images of UCNPs@mSiO2-Ir treated HeLa cells under 2.5% and 21% O2. e,f) Reproduced with permission.[84] Copyright 2015, John Wiley and Sons.

ADVANCED
SCIENCE NEWS
www.advancedsciencenews.com

NANO · MICRO
small
www.small-journal.com

time-resolved fluorescence immunoassay. These have included GdF$_3$:Tb,[49] NaYF$_4$:Ce/Tb,[46] ZrO$_2$:Tb,[83] and NaEuF$_4$ nanoparticles[48] for avidin and carcinoembryonic antigen detection. Due to their bright luminescence and long luminescence lifetime, these DSNPs probes achieved background-free high-sensitive detection.

DSNPs have also been applied for detection of cells and intercellular molecules. Huang and co-workers constructed the core–shell nanoparticles, NaYF$_4$:Yb,Tm@NaYF$_4$@mSiO$_2$-Ir, with a lanthanide-doped core and a mesoporous silica shell loaded with iridium(III) complex.[84] These core–shell nanoparticles could be excited at 450 nm with emission at 600 nm. Because the emission intensity at 600 nm was quenched by oxygen, the nanoparticles could be utilized as a probe for monitoring the oxygen concentration in living cells (Figure 8e). To achieve autofluorescence-free intracellular oxygen sensing, time-resolved luminescence imaging technology was adopted in this work to monitor oxygen levels in HeLa cells (Figure 8f). Photoluminescence lifetime imaging microscopy (PLIM) images showed that the emission lifetime in cells with 2.5% oxygen concentration was longer than that with 21% oxygen concentration. Time-gated luminescence images also displayed stronger signals with 2.5% O$_2$ as compared to the signals with 21% O$_2$. Thus, the change in intracellular O$_2$ concentration could be detected by the core–shell probe via time-resolved luminescence imaging technology. Moreover, a cover glass was used to cover the tops of cultured cells to oxygen concentration gradient for further monitoring. The intensity of luminescence was enhanced and the luminescence lifetime was increased with decreasing oxygen concentration from the edge to the center of the slide. The oxygen concentrations at the center, in the middle, and on the edge of slide, were 2.5%, 10%, and 21%, respectively. Due to the highly sensitive oxygen sensing performance, the oxygen probe shows promise for application in biomedical fields.

5.3. Lanthanide-Doped Downshifting Nanoparticles for Time-Resolved In Vivo Bioimaging

In the past decades, many kinds of luminescent probes, including fluorescent proteins, organic dyes, and luminescent nanoparticles have been employed for bioimaging.[86–88] When it comes to in vivo imaging, autofluorescence and light scattering must be taken into consideration.[89–91] Time-resolved imaging technique has become a useful method for complete removal of autofluorescence especially using lanthanide-doped DSNPs having long luminescence lifetimes. Moreover, NIR-to-NIR lanthanide-doped downshifting nanoparticles have been fabricated and used for autofluorescence-free deep tissue bioimaging via time-resolved imaging technique.

Jaque and co-workers synthesized Nd-doped DSNPs and used them as probe for in vivo imaging via time-gated imaging technique.[91] In their work, the NaGdF$_4$:Nd were prepared using a thermal decomposition method. The prepared DSNPs showed NIR emission bands centered at around 850, 1060, and 1350 nm under 808 nm laser excitation. The luminescence lifetime at 1060 nm was 90 µs, making NaGdF$_4$:Nd promising probes for background-free imaging via time-gated imaging technique. The time-gated imaging system was designed by

modifying the existing NIR in vivo imaging systems with a pulsed 808 nm laser, a "trigger delay" electronic circuit and an InGaAs camera (**Figure 9**a). The NaGdF$_4$:Nd nanoprobes were subcutaneously injected into the backs of mice or orally administered into the stomach. For subcutaneously injected mice, the images acquired without delay displayed strong autofluorescence, whereas the time-gated image obtained with 1 µs delay showed no autofluorescence (Figure 9b). The same result was obtained for the luminescence images of the oral administration group (Figure 9c). These results indicated that NaGdF$_4$:Nd nanoparticles were ideal long-lived probes for time-gated imaging to achieve background-free in vivo imaging with deep penetration, high contrast, and high resolution.

Lanthanide-doped DSNPs have been used for targeted cancer bioimaging. Zhang and co-workers designed a series of long-lived nanoparticles with lifetimes of several microseconds to several milliseconds for cancer imaging.[80] In their work, nanoparticles with core–multiple shell structure, NaGdF$_4$@NaGdF$_4$:Yb,Er@NaYF$_4$:Yb@NaNdF$_4$:Yb, were prepared, and the luminescence lifetime was tuned by changing the thickness of energy relay layer (NaYF$_4$:Yb) and varying the Er^{3+} concentration. Three lifetime populations of nanoparticles (Er–τ5, Er–τ9, and Er–τ13) were chosen as the probes (Figure 9d). These nanoparticles were conjugated with antibodies against different biomarkers of breast cancer (Er–τ5–antioestrogen receptor (ER), Er–τ9–anti-progesterone receptor (PR) and Er–τ13–antihuman epidermal growth factor receptor-2 (HER2)). The antibody-conjugated nanoparticles were further intravenously injected into nude mice bearing MCF-7 or BT-474 xenografted tumors. Background-free targeted tumor imaging was achieved with these long-lived probes via a time-resolved imaging system. In addition, this multiplexing method enabled the quantitative detection of biomarker expression in tumors by integrating the intensities of lifetime-resolved images (Figure 9e). Through this in vivo multiplexing method, the ratio of biomarker expression in MCF-7 tumors was determined to be 62.3% for ER, 17.9% for PR, and 19.8% for HER2. The ratio of biomarker expression in BT-474 tumors was 25.4% for ER, 28% for PR, and 46.6% for HER2. These expression results were highly consistent with the results of western blot and immunohistochemistry methods, demonstrating the excellent reliability of the in vivo multiplexing method. The in vivo multiplexing technology would contribute to wide range of biomedical and clinical applications, such as cancer diagnosis and therapy.

6. Lanthanide-Doped Persistent Luminescence Nanoparticles for Time-Resolved Biosensing and Bioimaging

Persistent luminescence nanoparticles (PLNPs) are special nanophosphors with luminescence decay time longer than several seconds, even up to several months.[92–94] In contrast to the above described lanthanide-doped UCNPs and DSNPs whose long lifetimes originate from the f–f forbidden transitions of lanthanides, the ultralong decay time of PLNPs is due to the capture and storage of excited charge carriers by the charged defects in PLNPs crystal lattice. It is generally accepted that PLNPs can
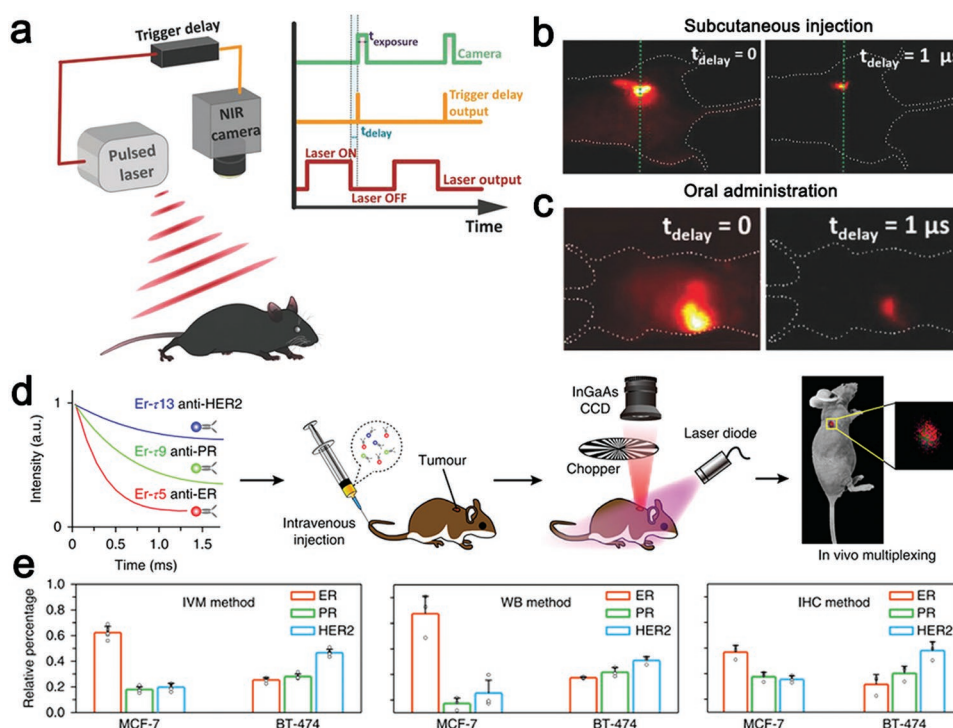
Figure 9. a) Schematic illustration of a time-gated imaging system for eliminating autofluorescence. b) Non-time-gated images (left) and time-gated images (right) of mouse subcutaneously injected with NaGdF$_4$:Nd nanoparticles. c) Non-time-gated images (left) and time-gated images (right) of mouse orally administered with NaGdF$_4$:Nd nanoparticles. a–c) Reproduced with permission.[91] Copyright 2015, John Wiley and Sons. d) Schematics illustrating the in vivo multiplexing method with three bioprobes exhibiting distinct lifetimes. e) Quantification of biomarker expression by in vivo multiplexing (IVM), western blot (WB), and immunohistochemistry (IHC) method. d,e) Reproduced with permission.[80] Copyright 2018, Springer Nature.

store excitation light energy in charged defects under excitation and further slowly release the energy to emitters to generate persistent luminescence after excitation ceases. Since the persistent luminescence can last for several hours or even tens of days, background signals including autofluorescence and scattered light can be easily eliminated by collecting the persistent luminescence signal after the background signals decay completely.[17,95] It is noteworthy that the complicated time-gated instruments involved in time-resolved analysis with lanthanide-doped UCNPs and DSNPs are not necessary for time-resolved analysis with PLNPs due to their ultralong decay times. In addition to efficient elimination of background signals, PLNPs are ideal for biotracing and long-term bioimaging with their long-lived luminescence, making PLNPs highly valuable in deciphering the functions of biomolecules and the behavior of biological systems.

Due to their abundant energy levels, lanthanides have been doped in PLNPs to serve as the sensitizers or emitters to realize persistent emissions ranging from UV to NIR regions. In the past decade, different kinds of lanthanide-doped PLNPs have been developed and their biomedical applications have been largely explored, such as in α-fetoprotein and ascorbic acid detection as well as targeted tumor imaging.[96–101] Moreover, vis-to-NIR or NIR-to-NIR lanthanide-doped PLNPs that can be repeatedly charged in vivo have been developed for achievement of deep tissue and long-term bioimaging.[93,102–104] Due to these unique properties, lanthanide-doped PLNPs have become ideal probes for highly sensitive biosensing and high resolution bioimaging.

6.1. Strategies for Tuning the Decay Time and Intensity of Persistent Luminescence

Developing PLNPs with enhanced persistent luminescence intensity and prolonged decay time can contribute to sensing and imaging with high signal-to-noise ratio. Charged defects play a crucial role in the generation of persistent luminescence, which can store the charge carriers and then gradually release them to produce persistent luminescence. The intensity and decay time of persistent luminescence are dominated by the amount and depth of defects, which serve to tune the persistent luminescence in PLNPs.[92] There are several strategies to introduce charged defects into crystal lattices, including varied the ratio of reactants to form nonstoichiometric defects, heterovalence ion doping to produce substitutional defects and high temperature calcination to generate surface oxygen vacancies.[102,103,105–108]

In 2012, Bessière and co-workers prepared the NIR persistent luminescence phosphor, ZnGa$_2$O$_4$:Cr and demonstrated that the decay time of persistent phosphors can be tuned by changing the stoichiometric ratio of the metal ion.[102] In their work, three kinds of ZnGa$_2$O$_4$:Cr phosphors were prepared, Zn$_{0.99}$Ga$_{1.99}$Cr$_{0.01}$O$_4$ (Zn-deficient compound), ZnGa$_{1.99}$Cr$_{0.01}$O$_4$ (stoichiometric compound), and Zn$_{1.01}$Ga$_{1.99}$Cr$_{0.01}$O$_4$ (Zn-excess compound). The three kinds of persistent luminescence phosphors showed NIR emission at 695 nm with excitation at 247 nm. For the emission spectra, several emission lines, N2 line (N2 zero photon line) and R lines (Stokes phonon sideband

ADVANCED
SCIENCE NEWS
www.advancedsciencenews.com

NANO · MICRO
small
www.small-journal.com

lines) can be observed. The N2 line is responsible for the persistent luminescence of $ZnGa_2O_4$:Cr phosphors. In the emission spectra of the three compounds, the intensity ratio of the N2 line to the R lines increased from the Zn-deficient compound toward the Zn-excess compound. The increased intensity ratio of the N2/R lines can be ascribed to the increased presence of charged defects in the Zn-excess compound as the Zn/Ga nominal ratio increases.

Richard and co-worker developed a lanthanide ion-doping strategy to control the electron trap depth for tuning the persistent luminescence properties in $CaMgSi_2O_6$:Mn.[108] In their work, four kinds of $CaMgSi_2O_6$:Mn,Ln (Ln = Dy, Pr, Ce, Nd) nanoparticles showing persistent luminescence at 685 nm under X-ray excitation were prepared. They exhibited similar persistent luminescence decay with $CaMgSi_2O_6$:Mn,Pr PLNPs displaying the most intense persistent luminescence. Thermally stimulated luminescence (TSL) measurements showed that $CaMgSi_2O_6$:Mn,Pr exhibits a strong TSL peak centered at 353 K, which is located at the proper temperature range for room temperature persistent luminescence. The other three kinds of PLNPs possessed TSL peaks located outside the proper temperature range. Thus Pr^{3+} was the most suitable Ln^{3+} to form the optimal electron trap depth in the crystal lattice, and the incorporation of Pr^{3+} into $CaMgSi_2O_6$:Mn led to the most intense persistent luminescence in $CaMgSi_2O_6$:Mn,Pr.

Recently, our group showed that heterovalence doping is a potent method to tune persistent luminescence intensity and decay time in PLNPs. In our work, Ge^{4+} was used as the co-dopant to tune the persistent luminesce properties of $ZnGa_2O_4$:Cr.[103] Six kinds of PLNPs, $Zn_{1+x}Ga_{2-2x}Ge_xO_4$:Cr(x = 0–0.5) were directly synthesized via a hydrothermal method. The sizes of the $Zn_{1+x}Ga_{2-2x}Ge_xO_4$:Cr nanoparticles increased from about 7 nm to around 80 nm with increasing x (**Figure 10**a). These PLNPs could be activated by a wide range of excitation sources in the UV and visible regions and exhibited NIR emission centered at around 700 nm (Figure 10b). The intensity and decay time of persistent luminescence in $Zn_{1+x}Ga_{2-2x}Ge_xO_4$:Cr nanoparticles were fine-tuned by changing the doping amount of Ge^{4+} (Figure 10c). All of the $Zn_{1+x}Ga_{2-2x}Ge_xO_4$:Cr nanoparticles displayed bright luminescence and long decay time, and the composition with x = 0.2 exhibited the longest persistent luminescence decay time of more than 10 h. The mechanism of the fine-tuned persistent luminescence in $Zn_{1+x}Ga_{2-2x}Ge_xO_4$:Cr was further studied.[107] Rietveld refinements demonstrated that Ge^{4+} was substituted into the octahedral Ga^{3+} sites, which led to cosubstitution of Ga^{3+} by Zn^{2+} for charge compensation (Figure 10d). Due to the similar electronic structure and size between Ge^{4+}, Ga^{3+}, and Zn^{2+}, a large amount of Ge^{4+} ions can enter the lattice of $ZnGa_2O_4$, introducing large amounts of charged defects in the host lattice (Figure 10e). The increase of charged defects led to significantly enhanced persistent luminescence intensity and prolonged decay time. However, excessive defects were deleterious and resulted in cross-relaxation between nearby defects, leading to quenching of persistent luminescence. Therefore, to achieve the strongest persistent luminescence, an optimal density of charged defects in $Zn_{1+x}Ga_{2-2x}Ge_xO_4$:Cr PLNPs is needed. These results showed that hetero-valence ion doping strategy is a potent strategy to fine tune the persistent luminescence of PLNPs.

6.2. Lanthanide-Doped Persistent Luminescence Nanoparticles for Time-Resolved In Vitro Biosensing

Due to their desirable properties, including ultralong persistent luminescence decay time and free of in situ excitation, PLNPs display obvious advantages in biosensing.[17,18] The persistent luminescence can last for hours to days, allowing the elimination of autofluorescence interference from complex biosamples. More importantly, the persistent luminescence collecting process does not require complex instruments. Measurements can be performed on a fluorescence spectrophotometer, microplate readers, or confocal microscopes. Sine in situ excitation is not needed for the sensing process, background noise resulting from excitation can also be avoided. Consequently, the signal-to-noise ratio of detection can be largely improved. Furthermore, with the recently developed "bottom-up" strategies for controlled synthesis of PLNPs, well-dispersed PLNPs with uniform size/shape and easy surface-functionalization have been prepared, increasing the convenience of designing PLNPs probes with conjugated targeting molecules. In recent years, lanthanide-doped PLNPs probes have been designed and their advantages in biosensing have been demonstrated.[96–101]

Yan and co-workers designed a fluorescence resonance energy transfer inhibition assay for highly selective and sensitive detection of α-fetoprotein based on $Ca_{1.86}Mg_{0.14}ZnSi_2O_7$:Eu,Dy and Au nanoparticles.[96] In their design (**Figure 11**a), the PLNPs and AuNPs were functionalized with polyethyleneimine (PEI) and an antibody (Ab) of α-fetoprotein, respectively. The positively charged PEI-PLNPs were bound via electrostatic interactions to the negatively charged Ab-AuNPs to form the FRET inhibition probe PEI-PLNPs/Ab-AuNPs. The PEI-PLNPs were illuminated with a UV lamp for 10 min to produce persistent luminescence before the detection. Because the absorption spectra of Ab-AuNPs overlaps the persistent luminescence emission spectra of PEI-PLNPs, FRET occurred, and the persistent luminescence of PEI-PLNPs was quenched. In the presence of AFP, Ab-AuNPs bond specifically to AFP and desorbed from PEI-PLNPs, leading to the recovery of persistent luminescence in PEI-PLNPs. The persistent luminescence intensity gradually increased with increasing AFP concentration in PBS buffer (Figure 11b). A linear range of detection from 0.8 to 45.0 µg L^{-1} was observed (Figure 11c) with a low detection limit of 0.41 µg L^{-1} AFP. The PEI-PLNPs/Ab-AuNPs probe was further successfully applied to AFP detection in human serum samples. The background interference from the serum samples was effectively eliminated by time-resolved analysis based on the long decay time of PLNPs. The serum AFP detection results were in good agreement with those obtained by enzyme-linked immunosorbent assay, clearly showing the good reliability and sensitivity of the time-resolved assay with PLNPs.

Tang and co-workers also developed an FRET inhibition assay for ascorbic acid detection.[97] In their work, CoOOH-modified $Sr_2MgSi_2O_7$:Eu,Dy PLNPs were used as the probe. Due to the good overlap of the emission band of PLNPs and the absorption band of CoOOH nanoflakes, the stored energy could be transferred from PLNPs to CoOOH nanoflakes via FRET, leading to efficiently quenched persistent luminescence from the probe. In the presence of ascorbic acid, the CoOOH nanoflakes were reduced to Co^{2+}, and the persistent luminescence of
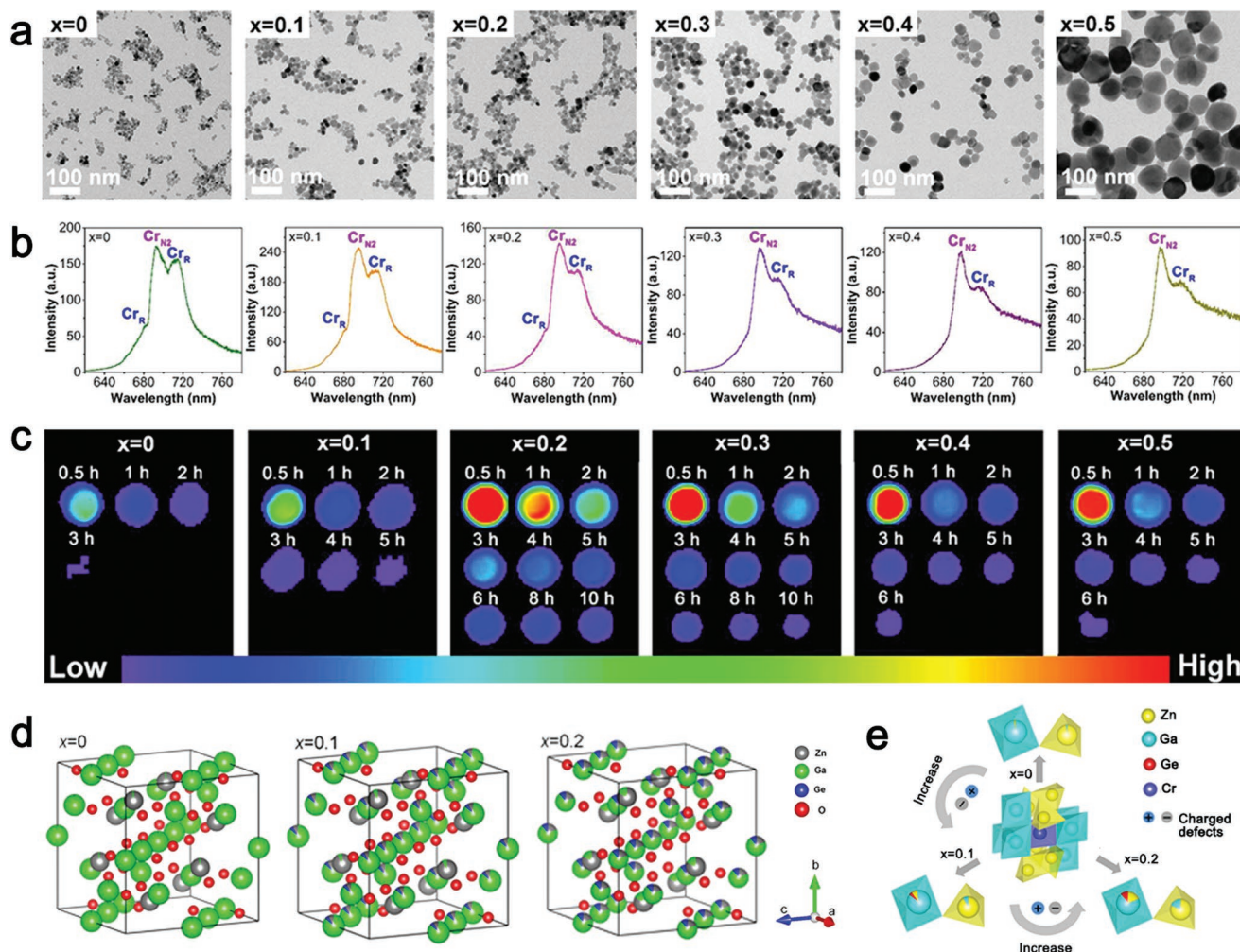
ADVANCED
SCIENCE NEWS
www.advancedsciencenews.com

NANO · MICRO
small
www.small-journal.com

Figure 10. a) TEM images of $Zn_{1+x}Ga_{2-2x}Ge_xO_4$:Cr ($x = 0$–0.5) nanoparticles. b) Photoluminescence spectrum and c) persistent luminescence decay images of the $Zn_{1+x}Ga_{2-2x}Ge_xO_4$:Cr ($x = 0$–0.5). a–c) Reproduced with permission.[103] Copyright 2017, American Chemical Society. d) The atom positions in the $Zn_{1+x}Ga_{2-2x}Ge_xO_4$:Cr ($x = 0$–0.2). e) Scheme of increased charged defects in $Zn_{1+x}Ga_{2-2x}Ge_xO_4$:Cr ($x = 0$–0.2) induced by Ge^{4+} doping. d,e) Reproduced with permission.[107] Copyright 2018, Springer Nature.

PLNPs was recovered (Figure 11d). When adding CoOOH-modified PLNPs to aqueous solutions containing increasing concentrations of ascorbic acid, the CoOOH-modified PLNPs showed enhanced persistent luminescence recovery (Figure 11e). A linear correlation between persistent luminescence intensity and ascorbic acid concentrations in the range from 1×10^{-6} to 100×10^{-6} M was observed (Figure 11f). The detection limit was determined to be 0.59×10^{-6} M. The inhibition nanoprobe was further applied for background-free detection of ascorbic acid in cell extracts and living cells. The results demonstrated that the FRET inhibition detection method using CoOOH-modified PLNPs as nanoprobe could effectively eliminate autofluorescence and realize highly sensitive biomolecule sensing. The Tang's group also prepared MnO_2-modified $Sr_2MgSi_2O_7$:Eu,Dy PLNPs as an inhibition probe for glutathione detection through a similar method.[98] A good linear relationship between persistent luminescence intensity and glutathione concentration was obtained with a low detection limit of 0.83×10^{-6} M. The nanoprobe was further used to detect glutathione in

mouse model. Background-free images were obtained due to the capability of the probe to eliminate autofluorescence and light scattering interference from biological samples.

Ju and co-workers developed a TR-FRET platform for intracellular caspase-3 detection (Figure 11g).[100] The $Sr_{1.6}Mg_{0.3}Zn_{1.1}Si_2O_7$:Eu,Dy PLNPs were functionalized with a cyclic arginine–glycine–aspartic acid peptide and FITC-labeled caspase-specific peptide. The persistent luminescence of PLNPs at 468 nm was quenched and the fluorescence intensity of FITC at 520 nm was enhanced due to FRET. Caspase-3 would cleave the caspase-specific peptide and release FITC, leading to dissociation of the FERT system. Thus, the emission of PLNPs increased and the emission of FITC decreased in the presence caspase-3. The long persistent luminescence of PLNPs was collected by time-resolved luminescence technique while the interference of short-lived FITC and autofluorescence was efficiently suppressed. For sensing in caspase assay buffer, the ratio of F468/F520 was used to quantify the concentration of caspase-3 and a linear detection range of caspase-3
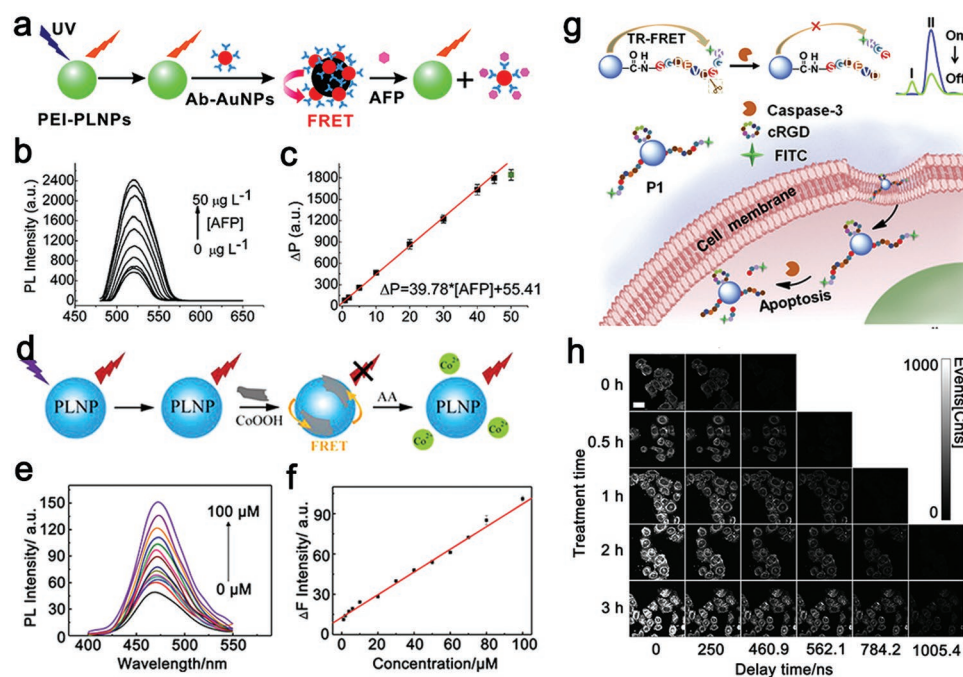
Figure 11. a) Scheme of the FRET inhibition assay for AFP detection. b) Persistent luminescence emission spectra of the PEI-PLNPs/Ab-AuNPs probe in the presence of different concentrations of AFP. c) Plot of enhanced persistent luminescence intensity (ΔP) against AFP concentration over the linear range from 0.8 to 45.0 µg L^{-1}. a–c) Reproduced with permission.[96] Copyright 2011, American Chemical Society. d) The design of CoOOH-modified PLNPs probe for AA detection. e) Persistent luminescence emission spectra of CoOOH-modified PLNPs exposed to different concentrations of AA in aqueous solution. f) Plot of enhanced persistent luminescence intensity (ΔF) against AA concentration over the linear range from 1×10^{-6} to 100×10^{-6} M. d–f) Reproduced with permission.[97] Copyright 2014, American Chemical Society. g) Schematic illustration of TR-FRET detection of caspase-3 based on a peptide-modified PLNPs probe. h) Fluorescence lifetime images of probe-labeled HeLa cells treated with apoptosis inducer for different times at different delay times. g,h) Reproduced with permission.[100] Copyright 2015, Elsevier.

from 1.0×10^{-4} to 10 unit mL^{-1} was obtained with a low detection limit of 2.4×10^{-5} unit mL^{-1}. For intracellular sensing, in situ detection of caspase-3 activity in live cells was realized with the PLNPs probe via time-resolved imaging microscopy (Figure 11h). An apoptosis inducer, cisplatin, was used to trigger the apoptosis in HeLa cell. The probe-treated HeLa cells showed brighter images with longer apoptosis inducer treatment time, indicating the increase amount of caspase-3 in HeLa cells. In addition, lifetime images obtained at different delay times showed the evolution of cell apoptosis. The PLNPs-based TR-FRET strategy can pave a new way for the design of sensitive detection methods, and further contribute to the dynamic tracking of the change of biomolecules in vivo.

6.3. Lanthanide-Doped Persistent Luminescence Nanoparticles for Time-Resolved Bioimaging

In 2007, Scherman and co-workers first used persistent luminescence nanoparticles for mouse imaging and demonstrated that PLNPs could effectively eliminate the autofluorescence interference.[109] Since then, PLNPs have attracted enormous attention in autofluorescence-free bioimaging. Since PLNPs exhibit long persistent luminescence after excitation ceases, autofluorescence-free imaging can be achieved by collecting the persistent luminescence signal. In addition, when PLNPs are used as probes, *in situ* excitation is not needed, leading to

minimal light scattering interference and phototoxicity. The first generation of PLNPs needed to be excited by UV light, which limited their applications in in vivo long-term bioimaging. In order to solve the problem, visible light activatable PLNPs and lanthanide-doped upconversion PLNPs have been developed. Compared with UV light, visible light can achieve deeper tissue penetration and less phototoxicity. Thus, visible light activatable PLNPs can be reactivated in vivo and are suitable for long-term bioimaging.[94,103] Recently, lanthanide-doped upconversion PLNPs that can be activated with 980 nm laser have been developed. The PLNPs can be repeatedly excited in vivo, enabling long-term bioimaging with high signal-noise ratio, minimal phototoxicity and deep tissue penetration.[104,105,110]

In 2014, Yan and co-workers fabricated a nanoprobe, $Zn_{2.94}Ga_{1.96}Ge_2O_{10}$:Cr,Pr PLNPs functionalized with gadolinium complexes, (Gd(III)-PLNPs), for in vivo multimode imaging.[111] The probe has an emission band at around 700 nm and persistent luminescence decay time of 30 h. The probes were used for small animal imaging by intravenous injection into nude mice. After removing the excitation, the persistent luminescence signal could be collected for more than 6 h (**Figure 12**a), indicating that the probe was suitable for long-term in vivo imaging. They also used the probe for magnetic resonance imaging (MRI) of Kunming mice. The probe showed an enhanced MRI signal in the liver site with high spatial resolution. The strategy of combining PLNPs with other functional materials could promote the development of multimode
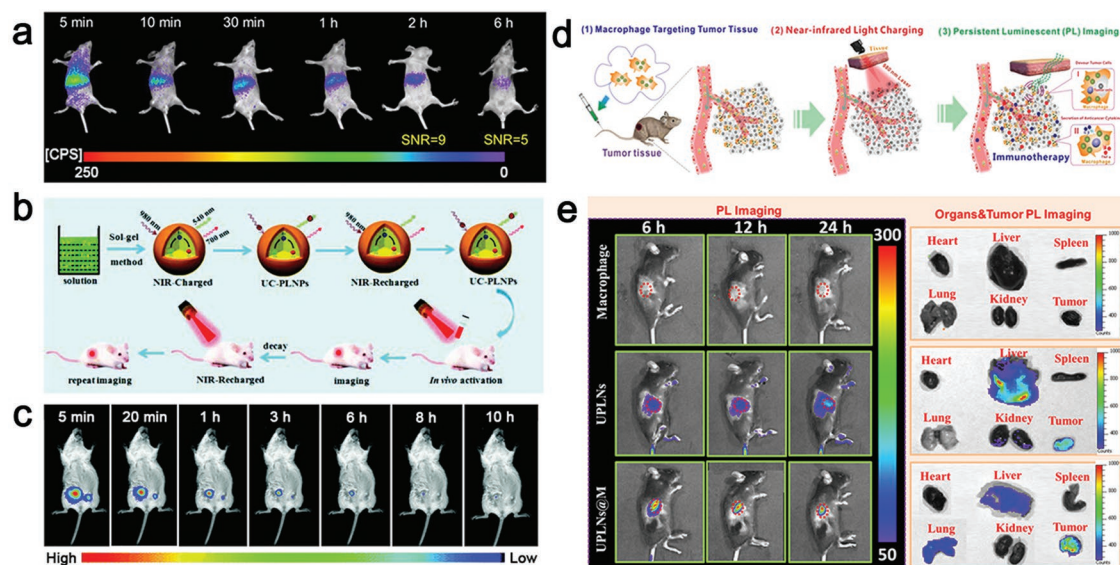
ADVANCED
SCIENCE NEWS
www.advancedsciencenews.com

NANO · MICRO
small
www.small-journal.com

Figure 12. a) In vivo persistent luminescence images of normal mouse intravenously injected with Gd(III)-PLNPs. Reproduced with permission.[111] Copyright 2014, American Chemical Society. b) Schematic representation of preparation of rechargeable NIR-to-NIR $Zn_3Ga_2GeO_8$:Cr,Yb,Er nanoparticles for in vivo bioimaging. c) In vivo upconversion persistent luminescence images of mouse subcutaneously injected with $Zn_3Ga_2GeO_8$:Cr,Yb,Er. a–c) Reproduced with permission.[105] Copyright 2017, Royal Society of Chemistry. d) Scheme of UPLNs@M probe for imaging-guided cell therapy in vivo. e) Upconversion persistent luminescence images of tumor-bearing mice after subcutaneous injection with macrophage, UPLNs, and UPLNs@M, as well as the persistent luminescence images of organs and tumors of the corresponding mice. d,e) Reproduced with permission.[110] Copyright 2018, American Chemical Society.

in vivo imaging system with high sensitivity and high spatial resolution.

In another work, Zhang and co-workers prepared an NIR nanoprobe for long-term tumor monitoring.[112] The $Zn_{1.1}Ga_{1.8}Ge_{0.1}O_4$:Cr,Eu@SiO$_2$ PLNPs showed NIR emission at 696 nm. The decay time of the PLNPs exceeded 15 days, making them suitable for long-term bioimaging. The PLNPs were functionalized with folic acid and then intravenously injected into tumor-bearing mice. A strong persistent luminescence signal was observed at the tumor site, suggesting the excellent tumor-targeting capacity of the probe. More importantly, the probe can be reactivated using a red LED lamp. A clear persistent luminescence signal at the tumor site was recovered after excitation with the LED lamp. These results demonstrated that the nanoprobe has excellent capacity for real-time monitoring of tumor in vivo.

Recently, NIR-to-NIR PLNPs with upconversion persistent luminescence have been designed for in vivo bioimaging. Because these new PLNPs can be in situ and repeatedly excited with 980 nm excitation, they are ideal for autofluorescence-free and long-term bioimaging. Li and co-workers designed upconversion persistent luminescence nanocomposites composed of upconversion nanoparticles and persistent luminescence nanoparticles.[104] In their design, the excitation energy could be absorbed by UCNPs and then transferred to PLNPs, leading to the generation of persistent luminescence. The UC-PLNPs were prepared via evaporation-induced self-assembly of β-NaYbF$_4$:Tm@NaYF$_4$ UCNPs and $Zn_{1.1}Ga_{1.8}Ge_{0.1}O_4$:Cr PLNPs. The resulting UC-PLNPs could be activated with a 980 nm laser and showed an emission band at 700 nm. Background-free and highly sensitive imaging of lymphatic nodes on nude mice was achieved using the UC-PLNPs probes. In another work, Zeng

and co-workers developed 980 nm laser-activated UC-PLNPs ($Zn_3Ga_2GeO_8$:Cr,Yb,Er) by integrating upconversion luminescence and persistent luminescence in a single host.[105] In the UC-PLNPs (Figure 12b), Yb^{3+} absorbed the excitation energy and transferred it to Er^{3+}, leading to the characteristic green emission of Er^{3+}. The energy could be further transferred to Cr^{3+}, resulting in NIR emission of Cr^{3+}. Both green and NIR emission could be observed under excitation with a 980 nm laser, while only NIR emission remained in the absence of excitation. The NIR excitation and NIR persistent luminescence properties made UC-PLNPs ideal probes for rechargeable in vivo bioimaging. Different concentrations of UC-PLNPs were subcutaneously injected into a mouse after preactivation for 10 min with a 980 nm laser. Strong persistent luminescence signal was detected in the mouse without any autofluorescence interference (Figure 12c). Notably, the signal could be observed even after 10 h, demonstrating that these UC-PLNPs would be ideal for long-term bioimaging. Importantly, the persistent luminescence can be easily renewable in vivo by the 980 nm laser. The UC-PLNPs preparation strategy proposed here could promote the development of PLNPs and further contribute to in vivo long-term bioimaging.

Chang and co-workers prepared NIR-excited Zn_2SiO_4:Mn,Y,Yb,Tm UC-PLNPs, and used the UC-PLNPs as probes for imaging-guided tumor therapy.[110] The UC-PLNPs could be excited by 980 nm light and showed green emission at 525 nm. Notably, the persistent luminescence could last for more than 40 min after excitation ceased, and the persistent luminescence could be recovered by repeated illumination with a 980 nm laser, indicating UC-PLNPs could be used for long-term bioimaging. The UC-PLNPs were incubated with tumor-associated macrophages, and internalized in macrophages to form UC-PLNPs loaded macrophages

(UPLNs@M), which could act as targeted imaging probes and cell therapy materials (Figure 12d). In this system, due to targeted tumor recognition ability of macrophages, UPLNs@M can accumulate in the tumor site, and the macrophages can kill cancer cells by specific phagocytes and secretion of cytokines. Therefore, the UPLNs@M can be used for imaging-guided cell therapy. UPLNs@M were further injected into tumor-bearing mice to test the targeted imaging ability. Compared with mice treated with macrophages or UPLNs, the UPLNs@M-treated group showed the most intense persistent luminescence signal in the tumor area (Figure 12e). Also, the UPLNs@M-treated group displayed more accumulation of UPLNs@M in the tumor sites as compared to other internal organs. Furthermore, the UPLNs@M showed excellent solid tumor inhibitory efficiency. These results demonstrated that UPLNs@M can be used for targeted recognition and imaging-guided cell therapy.

7. Lanthanide-Incorporated Polymer Nanoparticles for Time-Resolved Biosensing and Bioimaging

7.1. Lanthanide Coordination Polymer Nanoparticles for Time-Resolved Biosensing and Bioimaging

Lanthanide coordination polymer nanoparticles (LCPNs) form through self-assemble of organic bridging ligands and lanthanide ions.[113–115] In the LCPNs, the organic bridging ligands serve as antenna and the lanthanide ions act as chelators. Lanthanide ions endow LCPNs with unique properties, such as long fluorescence lifetimes, large Stokes shifts, and sharp emission bands, as well as nanosized pores and flexible structures. Due to these

excellent properties, LCPNs are suitable for background-free biosensing with time-resolved luminescence technology. Many kinds of LCPNs have been developed and widely employed in sensing targets varying from metal ions to biomolecules.[113–117]

Wu and co-workers developed a series of LCPNs based on guanosine 5′-monophosphate (GMP) and lanthanide ions (Tb^{3+} and Eu^{3+}) by varying the ratio of Tb^{3+}/Eu^{3+}.[117] The LCPNs were prepared by self-assembly of Tb^{3+} and Eu^{3+} with GMP (**Figure 13**a). In the nanoparticles, GMP can absorb excitation energy and transfer the energy to Tb^{3+} via ligand-to-metal energy transfer, leading to the characteristic green emission of Tb^{3+}. Also, the energy can be further transferred from Tb^{3+} to Eu^{3+} to give the characteristic red emission of Eu^{3+}. With the proposed energy transfer pathway, dual-emission luminescent nanomaterials have been obtained. Moreover, the relative intensity of the green and red emissions of LCPNs could be tuned by varying the concentrations of two lanthanides. As the Eu^{3+} concentration increased, the emission intensity of Tb^{3+} decreased and the emission intensity of Eu^{3+} increased. However, when the $Eu^{3+}:Tb^{3+}$ ratio became greater than 1:4, the emission of Eu^{3+} decrease and finally disappeared. Moreover, the lifetime of Tb^{3+} became shorter as Eu^{3+} content increased (Figure 13b), whereas the lifetime of Eu^{3+} increased initially and decreased afterward. Such LCPNs exhibit tunable long fluorescence lifetimes, making them suitable for highly sensitive sensing through time-resolved luminescence technique.

Chen and co-workers reported the synthesis of LCPNs for serum Fe^{2+} detection by the self-assembly of ligand 1,10-phenanthroline, lanthanide ion (Tb^{3+}) and nucleotide.[114] In the LCPNs, 1,10-phenanthroline served as sensitizer, which could absorb excitation energy at 265 nm
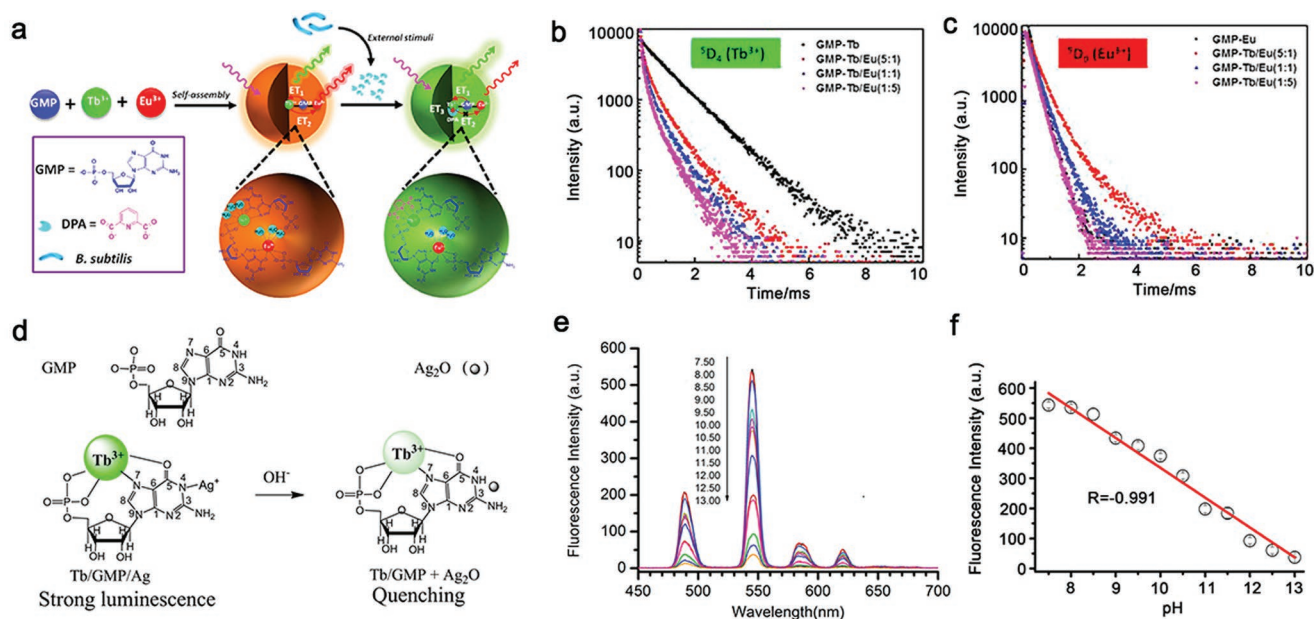

Figure 13. a) Scheme of the preparation of lanthanide coordination polymer nanoparticles GMP-Tb/Eu. b) Fluorescence decay curves of Tb^{3+} and c) Eu^{3+} in GMP-Tb/Eu with varying ratios of Tb^{3+}/Eu^{3+}. a–c) Reproduced with permission.[117] Copyright 2018, American Chemical Society. d) Principle of lanthanide-coordination polymer nanoparticle probe Tb/GMP/Ag for pH sensing. e) Fluorescence emission spectra of the probe in solutions with different pHs. f) Plot of fluorescence intensity at 543 nm versus pH value over the linear pH range of 7.5–13.0. d–f) Reproduced with permission.[114] Copyright 2017, Elsevier.

ADVANCED
SCIENCE NEWS
www.advancedsciencenews.com

NANO · MICRO
small
www.small-journal.com

and transfer it to Tb^{3+}, leading to green emission of Tb^{3+}. In the presence of Fe^{2+}, the $Fe(Phen)_3$ complex was formed and the LCPNs fluorescence was quenched. Because the LCPNs have a long lifetime of 1.042 ms, they could be used for autofluorescence-free detection of Fe^{2+} in human serum via time-resolved fluorimetry. A linear detection range of 80×10^{-9} M —to 6×10^{-3} M was achieved, which covers the concentration range of Fe^{2+} in human serum (11×10^{-6} to 29×10^{-6} M). Therefore, the LCPNs are suitable for highly sensitive sensing of bioactive compounds in serum without background interference.

For biosensing applications, water dispersible LCPNs are needed; thus, development of water dispersible LCPNs is of great importance. Xu and co-workers utilized GMP, lanthanide ions (Tb^{3+}), and silver ions (Ag^+) to prepare pH responsive LCPNs.[115] In the LCPNs, GMP served as a water-soluble bridging linker, Tb^{3+} acted as luminescent center, and Ag^+ was used as sensitizer for Tb^{3+} (Figure 13c). The LCPNs exhibited bright green emission at 545 nm under UV excitation. Because Ag^+ could bind to OH^- and precipitate as Ag_2O in alkaline solutions, the fluorescence of the LCPNs could be quenched by increasing the pH value. Based on the change of fluorescence in the presence of OH^-, the LCPNs could be used as a highly selectivity probe for OH^-. In addition, due to their long fluorescence lifetime of 0.86 ms, the LCPNs could be used as time-resolved fluorescence sensors to eliminate background fluorescence from biosamples. When employed for pH sensing in serum, the fluorescence intensity of probe gradually decreased with increasing pH (Figure 13d). In addition, the probe exhibited a broad pH detection range from 7.5 to 13. Moreover, the sensing result of pH obtained with LCPNs probe was comparable to that of a pH meter. The above works demonstrated that different structures of LCPNs could be designed for high-sensitive detection of ions/molecules.

7.2. Lanthanide Complex-Embedded Polymer Nanoparticles for Time-Resolved Biosensing and Bioimaging

The lanthanide complex-embedded polymer nanoparticles usually consist of a polymer matrice with embedded lanthanide complex. The polymer acts as a host matrice to disperse the lanthanide complex and as energy donor that can absorb excitation light and transfer the energy to the lanthanide complex to generate characteristic emission of lanthanide.[118–120] Lanthanide complexes are commonly used as fluorescence probe for sensing and imaging due to their long luminescence lifetimes, narrow emission bandwidths, large Stokes shifts, and bright luminescence. In the polymer matrix, the lanthanide complexes can retain their good optical properties and gain enhanced photostability. In addition, the polymer matrix can prevent leakage of lanthanide complexes, thereby reducing the toxicity in bioapplications. These properties make lanthanide complex-embedded polymer nanoparticles excellent candidates for biosensing and bioimaging.[60,117,121,122]

In 2013, Chiu and co-workers prepared polymer dots (Pdots) doped with an Eu^{3+} complex by a nanoprecipitation method and applied it for time-resolved cell labeling.[118] In the doped Pdots, poly(9-vinylcarbazole) (PVK) was chosen as the host matrix to disperse the Eu^{3+} complex (**Figure 14**a). Because the emission spectrum of PVK overlapped well with the excitation spectrum of the Eu^{3+} complex, PVK could transfer the absorbed energy to the Eu^{3+} complex through efficient FRET, leading to intense red emission at around 612 nm. The as-prepared Pdots displayed a sharp emission band of 8 nm and long fluorescence lifetime (hundreds of microseconds). Such long lifetime could distinguish the Pdots from other short-lived luminescence biomolecules via time-resolved imaging technique. Fluorescent nanoparticles (R300 NPs) with red emission at 612 nm were used as a short-lived background fluorescence substance to test the capability of the Pdots in eliminating background interference. Owing to the spectral overlap between R300 NPs and Pdots, the fluorescence signal of Pdots could not be distinguished from that of R300 NPs with a normal epifluorescence microscope (Figure 14b). When time-gated fluorescence microscopy was used, the short-lived background signal of R300 NPs disappeared rapidly and the long-lived fluorescence signal of Pdots was clearly obtained. The Pdots were further conjugated with the primary antibody of cell surface receptor EpCAM and were used to detect MCF-7 cells. Due to the capability of the probe to eliminate background florescence, cell imaging with high signal-to-noise was achieved.

The lanthanide complex-embedded polymer nanoparticles were also employed for time-resolved targeted tumor imaging. Wang and co-workers designed lanthanide complex-embedded polymer nanoparticles, Eu@SMA, based on $Eu(tta)_3bpt$ and poly(styrene-*co*-maleic acid) (SMA) for targeted tumor imaging.[122] In their design (Figure 14c), the Eu@SMA showed two-photon excitation, long luminescence lifetime, bright red luminescence, and good water dispersability. The bioprobe (Eu@SMA-Tf) was prepared by modifying Eu@SMA with a tumor-targeting unit, transferrin (Tf). The Eu@SMA-Tf was intravenously injected into tumor-bearing nude mice and the luminescence in the tumor sites was detected with two-photon excitation time-resolved imaging apparatus. The intravenous injection of Eu@SMA-Tf into normal mice without tumor was performed as the control. The tumor site showed stronger luminescence signal than that of the control (Figure 14d). Due to the long lifetime of the Eu@SMA-Tf probe, the autofluorescence interference was effectively suppressed by the two-photon excitation time-resolved imaging technique. The design strategy for the long-lived probe reported is an excellent example of the application of lanthanide complex-embedded polymer nanoparticles in areas such as medical diagnosis, biomedicine, and life science.

8. Lanthanide-Incorporated Silica Nanoparticles for Time-Resolved Biosensing and Bioimaging

Silica nanoparticles are also used as matrices for lanthanide ions and lanthanide complexes.[123–129] Because the synthesis of silica nanoparticles is simple, lanthanide-incorporated silica nanoparticles can be prepared easily. The good water dispersibility and biocompatibility of silica nanoparticles, are maintained
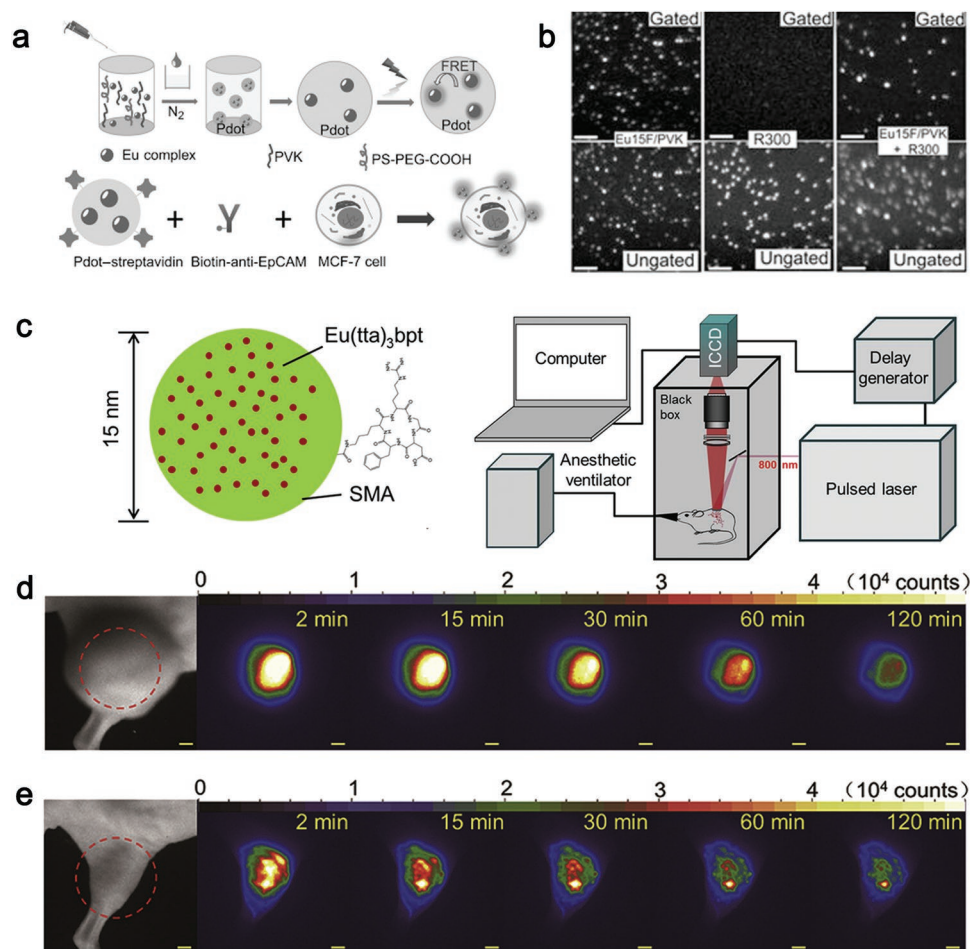
ADVANCED
SCIENCE NEWS
www.advancedsciencenews.com

NANO · MICRO
small
www.small-journal.com

Figure 14. a) Scheme of preparation and modification of Eu^{3+} complex-doped Pdots for cells labeling. b) Time-gated and ungated images of doped-Pdots, R300 nanoparticles, and mixtures of doped-Pdots and R300 nanoparticles, scale bar: 5 mm. a,b) Reproduced with permission.[118] Copyright 2013, John Wiley and Sons. c) Schematic representation of Eu^{3+} complex-embedded polymer Eu@SMA and the two-photon excitation time-resolved imaging apparatus. The time-resolved images of Eu@SMA-Tf treated d) tumor-bearing mice and e) normal mice. c–e) Reproduced with permission.[122] Copyright 2016, Elsevier.

in lanthanide-incorporated silica nanoparticles. In addition, silica encapsulation can prevent lanthanide luminescence from being quenched by the outside solvent and oxygen molecules. Thus lanthanide-incorporated silica nanoparticles have bright luminescence, good photostability, and long luminescence lifetimes. Furthermore, the silica matrix can prevent the leakage of lanthanides and thereby minimizing the potential toxicity in biosensing and bioimaging. Moreover, various functional molecules can be easily bonded on the surfaces of silica nanoparticles. In general, silica nanoparticles provide an ideal matrix for lanthanides, and the lanthanide-incorporated silica nanoparticles are suitable nanoprobes for biosensing and bioimaging.

Yoon and co-workers developed lanthanide complex-incorporated silica nanoparticles and utilized them as a time-resolved immunosensing probe for cardiac troponin I (cTnI) detection.[128] In their work, the lanthanide complex was covalently bonded to the silane monomer to form a lanthanide chelate–silane complex. The prepared Eu^{3+} complex was further crosslinked with silica precursors to obtain Eu^{3+} complex-incorporated silica nanoparticle (**Figure 15**a), which displayed characteristic Eu^{3+} emission at around 615 nm under 340 nm

illumination. The doped nanoparticles were further modified with anti-cTnI antibody and employed as probe for cardiac troponin I detection through sandwich-based time-resolved luminescence immunoassay (Figure 15a). The nanoprobe was used to detect different concentrations of cTnI (0, 0.05, 0.5, 1, 5, and 20 ng mL^{-1}) in PBS. After the removal of excitation light, time-resolved luminescence of the probe gradually decreased over time and the decay rate of photon counts decreased with increasing concentrations of cTnI (Figure 15b). By collecting time-resolved luminescence photon counts over 1 s, a good linear relationship between the integrated photon counts and the concentration of cTnI was observed. A linear detection range of 50 pg mL^{-1}–10 ng mL^{-1} and a detection limit of 48 pg mL^{-1} were obtained (Figure 15c). These results indicated that time-resolved luminescence immunoassay based on the probe could be used for highly sensitive cTnI detection and further for early diagnosis of acute myocardial infarction.

Zhang and co-workers reported a time-resolved ratiometric fluorescent probe for detecting an anthrax biomarker, dipicolinic acid (DPA).[129] The probe consisted of lanthanide-doped silica nanoparticle core (Tb/DPA@SiO$_2$) and lanthanide
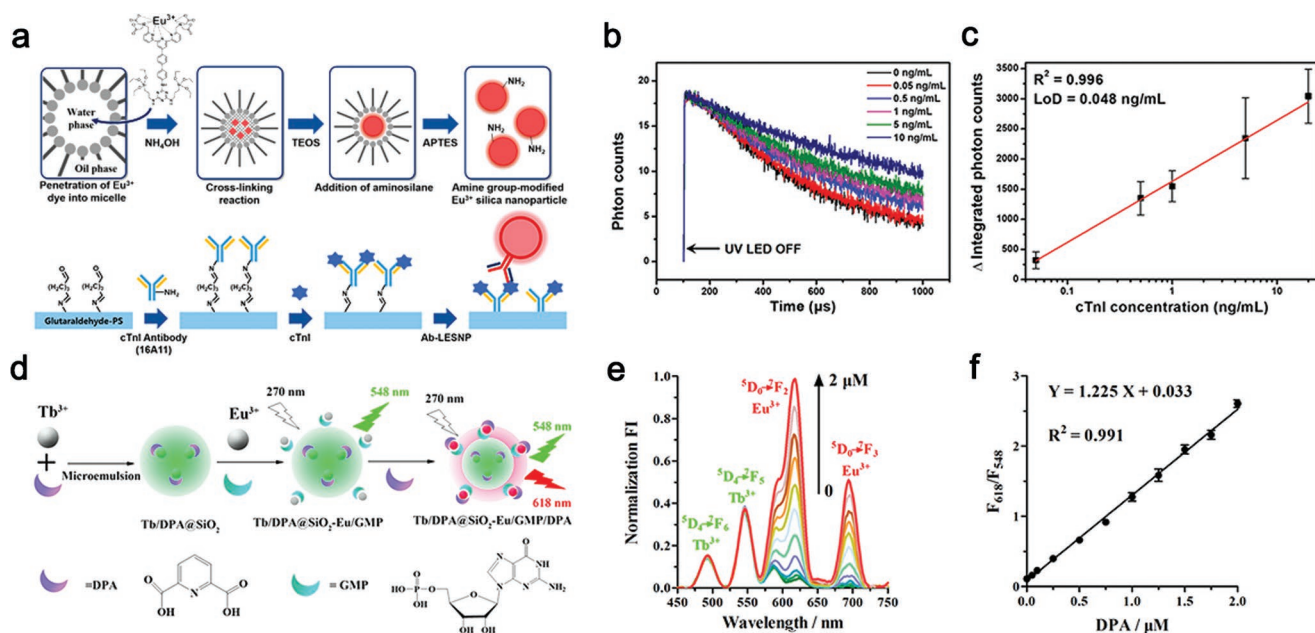
ADVANCED
SCIENCE NEWS
www.advancedsciencenews.com

NANO · MICRO
small
www.small-journal.com

Figure 15. a) Schematic illustrating the preparation procedures of Eu^{3+} complex-incorporated silica nanoparticles for time-resolved immunosensing of cTnI. b) Time-gated photon count curve of the probe in the presence of cTnI with different concentrations. c) Calibration curve of increased integrated photon counts versus cTnI concentration in the range of 50 pg mL^{-1}–10 ng mL^{-1}. a–c) Reproduced with permission.[128] Copyright 2017, MDPI. d) Schematic representation of the preparation of ratiometric fluorescent probe, Tb/DPA@SiO$_2$-Eu/GMP for DPA detection. e) Fluorescence emission spectra of the ratiometric fluorescent probe in the presence of DPA with different concentrations in Tris-HCl buffer. f) Plot of F618/F548 ratio versus the concentration of DPA over the linear range from 50×10^{-9} M to 2×10^{-6} M. d–f) Reproduced with permission.[129] Copyright 2017, Elsevier.

coordination polymer shell (Eu/GMP) (Figure 15d). In their design, DPA acted as energy-transfer donor for lanthanides. In the absence of DPA, the probe showed the green emission of Tb^{3+} under 270 nm excitation. Upon exposure to DPA, the probe emitted both the green fluorescence of Tb^{3+} and the red fluorescence of Eu^{3+}. Due to the core–shell structure, the changing concentration of DPA could affect only the outer red fluorescence, while the inner green fluorescence remained unchanged. Thus the green fluorescence could serve as internal reference signal, and the red fluorescence could act as response signal. In addition, the probe possessed long lifetime, which made it suitable for time-resolved fluorescence assays. The probe was used for DPA detection in Tris-HCl buffer. As the concentration of DPA increased, the fluorescence intensity at 618 nm increased, while the fluorescence intensity at 548 nm was almost constant (Figure 15e). A good linear relationship between the F618/F548 ratio and the concentrations of DPA was observed (Figure 15f). A linear range from 50×10^{-9} M to 2×10^{-6} M was obtained, and the detection limit reached 7.3×10^{-9} M. The probe was further embedded in filter paper to construct a paper-based visual sensor for DPA sensing. This work provided a potential method to construct time-resolved ratiometric fluorescent probes for sensitive and selective biomarker sensing, which would pave the way for the design of multifunctional probes for practical clinical applications.

9. Conclusion and Perspective

Owing to the unique electronic configuration of lanthanides, lanthanide-doped nanoparticles display many desirable properties, such as long luminescence lifetimes, large Stokes/anti-Stokes shifts, multiple emission bands, and narrow emission bandwidths. In addition, the tunable composition, size and shape of lanthanide-doped nanoparticles can be used to tune the luminescence properties. When lanthanide-doped nanoparticles are employed as long-lived probes for biosensing and bioimaging, the autofluorescence and light scattering interference can be completely avoided by collecting the long-lived luminescence signal after the background signal decays via time-resolved luminescence technique. Therefore, these excellent properties make lanthanide-doped nanoparticles widely employed in time-resolved bioapplications. As summarized in this review (**Table 1**), a variety of long-lived lanthanide-doped nanoparticles have been developed, including lanthanide-doped UCNPs, lanthanide-doped DSNPs, lanthanide-doped PLNPs, lanthanide-incorporated polymer nanoparticles and lanthanide-incorporated silica nanoparticles, and highly sensitive biosensing and high-contrast bioimaging have been achieved based on these long-lived lanthanide-doped nanoparticles.

In the future, the following aspects should be addressed to promote the application of lanthanide-doped nanoparticles in autofluorescence-free biomedical applications: (1) simple, cheap, and commercial time-resolved imaging system should be developed to facilitate the practical application of time-resolved luminescence analysis. Time-resolved luminescence analysis is an unparalleled analytical method that can completely eliminate background fluorescence interference and achieve zero background. It is important to promote the practical application of this analytical method. (2) Long-lived lanthanide-doped nanomaterials with prolonged lifetimes and enhanced intensity should be developed. As mentioned above,

Table 1. Lanthanide-doped nanoparticles used for time-resolved biosensing and bioimaging.

Lanthanide-doped nanoparticles	Luminescence lifetimes	Decay time	Detection target	Limit of detection	Ref.
$NaYF_4$:Yb(20%),Tm(1%)	160 μs		*Giardia lamblia*	Single *Giardia lamblia*	[63]
$NaYF_4$:Yb(20%),Tm(4%)	40 μs		*Giardia lamblia*	Single *Giardia lamblia*	[63]
$NaGdF_4$:Yb,Tm^{3+}@$NaYF_4$:Yb@$NaNdF_4$:Yb@$NaYF_4$	634 μs, 733 μs		HPV 16, HPV 18		[64]
$NaKYF_4$:Yb,Tm	260 μs		Biotin	3.0×10^{-9} M	[74]
CaF_2:Ce,Tb	12.5 ms		Biotin	48×10^{-12} M	[81]
CaF_2:Ce,Tb	12.5 ms		uPAR	328×10^{-12} M	[81]
GdF_3:Tb^{3+}	5.91 ms		Avidin	74×10^{-12} M	[49]
$NaYF_4$:Ce/Tb	2.21 ms		Avidin	4.8×10^{-9} M	[46]
ZrO_2:Tb^{3+}	1.82 ms		Avidin	3×10^{-9} M	[83]
$NaEuF_4$	2.16 ms		Carcinoembryonic antigen	0.5×10^{-15} M	[48]
$NaYF_4$:Yb,Tm@$NaYF_4$@$mSiO_2$-Ir	723 μs		Oxygen		[84]
$NaGdF_4$@$NaGdF_4$:Yb,Er@$NaYF_4$:Yb@$NaNdF_4$:Yb	0.55 ms, 1.73 ms, 7.21 ms		ER, PR, HER2	MCF-7 and BT-474 tumors	[80]
$Ca_{1.86}Mg_{0.14}ZnSi_2O_7$:Eu,Dy		6 h	α-Fetoprotein	0.41 μg L^{-1}	[96]
$Sr_2MgSi_2O_7$:Eu,Dy		more than 200 min	Ascorbic acid	0.59×10^{-6} M	[97]
$Sr_2MgSi_2O_7$:Eu,Dy		more than 200 min	Glutathione	0.83×10^{-6} M	[98]
$Sr_{1.6}Mg_{0.3}Zn_{1.1}Si_2O_7$:Eu,Dy		10 h	Caspase-3	2.4×10^{-5} unit mL^{-1}	[100]
$Zn_{1.1}Ga_{1.8}Ge_{0.1}O_4$:Cr,Eu@$SiO_2$		15 days	H22 tumor		[112]
Zn_2SiO_4:Mn,Y,Yb,Tm		more than 40 min	B16 tumor		[110]
LCPNs (Tb^{3+} doped)	1.042 ms		Serum Fe^{2+}		[114]
LCPNs (Tb^{3+},Ag^+ doped)	0.86 ms		pH		[115]
Pdots (Eu^{3+} complex doped)	509 μs, 202 μs		MCF-7 cells		[118]
Eu@SMA	620 μs		HepG-2 tumor		[122]
Silica NPs (Eu^{3+} complex doped)			Cardiac troponin I	48 pg mL^{-1}	[128]
Tb/DPA@SiO_2–Eu/GMP	191.62 μs		Dipicolinic acid	7.3×10^{-9} M	[129]

the collected luminescence signal of long-lived nanomaterials is usually weak after the background fluorescence disappears, so the signal collecting process needs to repeat many times to obtain good analysis results. Developing long-lived nanomaterials that can provide analysis result by a single signal collecting process is important. (3) Feasible strategies to prepare rechargeable NIR-to-NIR persistent luminescence nanoparticles, enhance their persistent luminescence, and prolong their decay time are also needed. PLNPs are ideal candidates for autofluorescence-free and long-term bioimaging due to their long persistent luminescence decay time. In addition, the complicated time-resolved imaging instruments are not necessary for time-resolved analysis with PLNPs. Rechargeable NIR-to-NIR PLNPs are suitable for biological processes tracking, and the enhanced persistent luminescence in these PLNPs can improve the sensitivity of detection and imaging.

The future development of the long-lived lanthanide-doped nanomaterials for time-resolved biosensing and bioimaging relies on the cooperation of materials scientists, analytical chemists and instrumentation experts in time-resolved luminescence analysis. In this way, biosensing with much higher sensitivity and bioimaging with much higher contrast can be achieved based on these long-lived lanthanide-doped nanoprobes via new time-resolved luminescence analysis systems.

Acknowledgements

Conflict of Interest

The authors declare no conflict of interest.

ADVANCED
SCIENCE NEWS

www.advancedsciencenews.com

NANO · MICRO
small
www.small-journal.com

Keywords

[1] E. Roduner, *Chem. Soc. Rev.* **2006**, *35*, 583.
[2] B. K. An, S. K. Kwon, S. D. Jung, S. Y. Park, *J. Am. Chem. Soc.* **2002**, *124*, 14410.
[3] J. Horyu, B. Geunchoi, J. Yoon, K. Boshim, K. Machi, K. Hamada, *J. Lumin.* **2007**, *124*, 67.
[4] N. E. Domracheva, V. E. Vorobeva, M. S. Gruzdev, A. V. Pyataev, *J. Nanopart. Res.* **2015**, *17*, 83.
[5] S. N. Baker, G. A. Baker, *Angew. Chem., Int. Ed.* **2010**, *49*, 6726.
[6] F. Wang, J. Wang, X. Liu, *Angew. Chem.* **2010**, *122*, 7618; *Angew. Chem., Int. Ed.* **2010**, *49*, 7456.
[7] L. Zhang, L. Yin, C. Wang, N. Lun, Y. Qi, D. Xiang, *J. Phys. Chem. C* **2010**, *114*, 9651.
[8] K. M. Mayer, J. H. Hafner, *Chem. Rev.* **2011**, *111*, 3828.
[9] K. L. Kelly, E. Coronado, L. Z. Lin, G. C. Schatz, *J. Phys. Chem. B* **2003**, *107*, 668.
[10] Y. Tian, B. Chen, Y. Mao, J. Sun, X. Li, J. Zhang, S. Fu, H. Zhong, B. Dong, X. Zhang, *J. Nanopart. Res.* **2013**, *15*, 1.
[11] Y. Sun, Y. Chen, L. Tian, Y. Yu, X. Kong, J. Zhao, H. Zhang, *Nanotechnology* **2007**, *18*, 447.
[12] N. Gao, Y. Chen, L. Li, Z. Guan, T. Zhao, N. Zhou, P. Yuan, S. Q. Yao, Q. H. Xu, *J. Phys. Chem. C* **2014**, *118*, 13904.
[13] X. Michalet, F. F. Pinaud, L. A. Bentolila, J. M. Tsay, S. Doose, J. J. Li, G. Sundaresan, A. M. Wu, S. S. Gambhir, S. Weiss, *Science* **2005**, *307*, 538.
[14] P. Wu, X. P. Yan, *Chem. Soc. Rev.* **2013**, *42*, 5489.
[15] F. Wang, Y. Han, C. S. Lim, Y. Lu, J. Wang, J. Xu, H. Chen, C. Zhang, M. Hong, X. Liu, *Nature* **2010**, *463*, 1061.
[16] J. Zhou, Z. Liu, F. Li, *Chem. Soc. Rev.* **2012**, *41*, 132.
[17] Y. Li, M. Gecevicius, J. Qiu, *Chem. Soc. Rev.* **2016**, *45*, 2090.
[18] J. Wang, Q. Ma, Y. Wang, H. Shen, Q. Yuan, *Nanoscale* **2017**, *9*, 6204.
[19] C. Wu, D. T. Chiu, *Angew. Chem., Int. Ed.* **2013**, *52*, 3086.
[20] A. Reisch, A. S. Klymchenko, *Small* **2016**, *12*, 1968.
[21] C. Geng, S. Xu, H. Zhong, A. L. Rogach, W. Bi, *Angew. Chem., Int. Ed.* **2018**, *57*, 9650.
[22] X. Li, F. Cao, D. Yu, J. Chen, Z. Sun, Y. Shen, Y. Zhu, L. Wang, Y. Wei, Y. Wu, *Small* **2017**, *13*, 1603996.
[23] Q. A. Akkerman, V. D'Innocenzo, S. Accornero, A. Scarpellini, A. Petrozza, M. Prato, L. Manna, *J. Am. Chem. Soc.* **2015**, *137*, 10276.
[24] J. Z. Song, J. H. Li, X. M. Li, L. M. Xu, Y. H. Dong, H. B. Zeng, *Adv. Mater.* **2015**, *27*, 7162.
[25] J. Z. Song, J. H. Li, L. M. Xu, J. H. Li, F. J. Zhang, B. N. Han, Q. S. Shan, H. B. Zeng, *Adv. Mater.* **2018**, *30*, 1800764.
[26] G. Xu, S. Zeng, B. Zhang, M. T. Swihart, K. T. Yong, P. N. Prasad, *Chem. Rev.* **2016**, *116*, 12234.
[27] T. Lécuyer, E. Teston, G. Ramirezgarcia, T. Maldiney, B. Viana, J. Seguin, N. Mignet, D. Scherman, C. Richard, *Theranostics* **2016**, *6*, 2488.
[28] G. Chen, H. Qiu, P. N. Prasad, X. Chen, *Chem. Rev.* **2014**, *114*, 5161.
[29] S. Fery-Forgues, *Nanoscale* **2013**, *5*, 8428.
[30] G. A. Mansoori, T. F. George, G. P. Zhang, L. Assoufid, *Molecular Building Blocks for Nanotechnology*, Springer, New York, NY, USA **2007**.
[31] N. L. Rosi, C. A. Mirkin, *Chem. Rev.* **2010**, *36*, 1547.
[32] M. E. Davis, Z. G. Chen, D. M. Shin, *Nat. Rev. Drug Discovery* **2008**, *7*, 771.
[33] Y. Matsumura, H. Maeda, *Cancer Res.* **1986**, *46*, 6387.
[34] A. M. Smith, M. C. Mancini, S. Nie, *Nat. Nanotechnol.* **2009**, *4*, 710.
[35] D. S. Richardson, J. F. Lichtman, *Cell* **2015**, *162*, 246.
[36] H. M. Kim, B. R. Cho, *Acc. Chem. Res.* **2009**, *42*, 863.
[37] S. Diao, G. Hong, A. L. Antaris, J. L. Blackburn, K. Cheng, Z. Cheng, H. Dai, *Nano Res.* **2015**, *8*, 3027.
[38] K. Suhling, P. M. W. French, D. Phillips, *Photochem. Photobiol. Sci.* **2005**, *4*, 13.
[39] K. Y. Zhang, Y. Qi, H. Wei, S. Liu, Z. Qiang, H. Wei, *Chem. Rev.* **2018**, *118*, 1770.
[40] J. Yuan, G. Wang, *TrAC Trends Anal. Chem.* **2006**, *25*, 490.
[41] V. Väisänen, H. Härmä, H. Lilja, A. Bjartell, *Luminescence* **2000**, *15*, 389.
[42] W. Zheng, D. Tu, P. Huang, S. Zhou, Z. Chen, X. Chen, *Chem. Commun.* **2015**, *51*, 4129.
[43] H. Shi, H. Sun, H. Yang, S. Liu, G. Jenkins, W. Feng, F. Li, Q. Zhao, B. Liu, W. Huang, *Adv. Funct. Mater.* **2013**, *23*, 3250.
[44] K. Y. Zhang, J. Zhang, Y. Liu, S. Liu, P. Zhang, Q. Zhao, Y. Tang, W. Huang, *Chem. Sci.* **2014**, *6*, 301.
[45] W. Lv, Z. Zhang, K. Y. Zhang, H. Yang, S. Liu, A. Xu, S. Guo, Q. Zhao, W. Huang, *Angew. Chem.* **2016**, *128*, 10101; *Angew. Chem., Int. Ed.* **2016**, *55*, 9947.
[46] D. Tu, L. Liu, Q. Ju, Y. Liu, H. Zhu, R. Li, X. Chen, *Angew. Chem.* **2011**, *123*, 6430; *Angew. Chem., Int. Ed.* **2011**, *50*, 6306.
[47] Y. Yang, D. Tu, W. Zheng, Y. Liu, P. Huang, E. Ma, R. Li, X. Chen, *Nanoscale* **2014**, *6*, 11098.
[48] S. Zhou, W. Zheng, Z. Chen, D. Tu, Y. Liu, E. Ma, R. Li, H. Zhu, M. Huang, X. Chen, *Angew. Chem.* **2014**, *126*, 12706; *Angew. Chem., Int. Ed.* **2015**, *53*, 12498.
[49] Q. Ju, Y. Liu, D. Tu, H. Zhu, R. Li, X. Chen, *Chem. - Eur. J.* **2011**, *17*, 8549.
[50] X. Chen, Y. Liu, D. Tu, *Lanthanide-Doped Luminescent Nanomaterials*, Springer, Berlin **2014**.
[51] F. Auzel, *Chem. Rev.* **2004**, *104*, 139.
[52] L. D. Sun, Y. F. Wang, C. H. Yan, *Acc. Chem. Res.* **2014**, *47*, 1001.
[53] H. Dong, S. R. Du, X. Y. Zheng, G. M. Lyu, L. D. Sun, L. D. Li, P. Z. Zhang, C. Zhang, C. H. Yan, *Chem. Rev.* **2015**, *115*, 10725.
[54] R. E. Connally, J. A. Piper, *Ann. N. Y. Acad. Sci.* **2008**, *1130*, 106.
[55] Z. Liao, M. Tropiano, K. Mantulnikovs, S. Faulkner, T. Vosch, T. J. Sørensen, *Chem. Commun.* **2014**, *51*, 2372.
[56] H. Zhang, J. Jiang, P. Gao, T. Yang, K. Y. Zhang, Z. Chen, S. Liu, W. Huang, Q. Zhao, *ACS Appl. Mater. Interfaces* **2018**, *10*, 17542.
[57] W. Zheng, P. Huang, D. Tu, E. Ma, H. Zhu, X. Chen, *Chem. Soc. Rev.* **2015**, *44*, 1379.
[58] S. Han, R. Deng, X. Xie, X. Liu, *Angew. Chem., Int. Ed.* **2014**, *53*, 11702.
[59] H. Dong, L. D. Sun, C. H. Yan, *Chem. Soc. Rev.* **2015**, *44*, 1608.
[60] J. C. Bünzli, *Acc. Chem. Res.* **2006**, *39*, 53.
[61] D. J. Garfield, N. J. Borys, S. M. Hamed, N. A. Torquato, C. A. Tajon, B. Tian, B. Shevitski, E. S. Barnard, Y. D. Suh, S. Aloni, *Nat. Photonics* **2018**, *12*, 402.
[62] B. Gu, Q. Zhang, *Adv. Sci.* **2018**, *5*, 1700609.
[63] Y. Lu, J. Zhao, R. Zhang, Y. Liu, D. Liu, E. M. Goldys, X. Yang, P. Xi, A. Sunna, J. Lu, Y. Shi, R. Leif, Y. Huo, J. Shen, J. Piper, J. Robinson, D. Jin, *Nat. Photonics* **2014**, *8*, 32.
[64] L. Zhou, Y. Fan, R. Wang, X. M. Li, L. L. Fan, F. Zhang, *Angew. Chem.* **2018**, *130*, 13006; *Angew. Chem., Int. Ed.* **2018**, *57*, 12824.
[65] H. Dong, L. D. Sun, L. D. Li, R. Si, R. Liu, C. H. Yan, *J. Am. Chem. Soc.* **2017**, *139*, 18492.

[66] A. Pilch, C. Würth, M. Kaiser, D. Wawrzyńczyk, M. Kurnatowska, S. Arabasz, K. Prorok, M. Samoć, W. Strek, U. Resch-Genger, A. Bednarkiewicz, *Small* **2017**, *13*, 1701635.

[67] H. Dong, L. D. Sun, W. Feng, Y. Gu, F. Li, C. H. Yan, *ACS Nano* **2017**, *11*, 3289.

[68] X. Liu, Y. Wang, X. Li, Z. Yi, R. Deng, L. Liang, X. Xie, D. T. B. Loong, S. Song, D. Fan, A. All, H. Zhang, L. Huang, X. G. Liu, *Nat. Commun.* **2017**, *8*, 899.

[69] X. Chen, L. Jin, T. Sun, W. Kong, S. F. Yu, F. Wang, *Small* **2017**, *13*, 1701479.

[70] L. Liu, S. Wang, B. Zhao, P. Pei, Y. Fan, X. Li, F. Zhang, *Angew. Chem., Int. Ed.* **2018**, *57*, 7518.

[71] M. K. Mahata, T. Koppe, T. Mondal, C. Brüsewitz, K. Kumar, R. V. Kumar, H. Hofsäss, U. Vetter, *Phys. Chem. Chem. Phys.* **2015**, *17*, 20741.

[72] L. Mattsson, K. D. Wegner, N. Hildebrandt, T. Soukka, *RSC Adv.* **2015**, *5*, 13270.

[73] M. C. D. Santos, N. Hildebrandt, *TrAC Trends Anal. Chem.* **2016**, *84*, 60.

[74] S. Lahtinen, Q. Wang, T. Soukka, *Anal. Chem.* **2016**, *88*, 653.

[75] L. Sun, R. Wei, J. Feng, H. Zhang, *Coord. Chem. Rev.* **2018**, *364*, 10.

[76] X. Zheng, X. Zhu, Y. Lu, J. Zhao, F. Wei, G. Jia, W. Fan, F. Li, D. Jin, *Anal. Chem.* **2016**, *88*, 3449.

[77] G. Chen, T. Y. Ohulchanskyy, S. Liu, W. C. Law, F. Wu, M. T. Swihart, H. Agren, P. N. Prasad, *ACS Nano* **2012**, *6*, 2969.

[78] S. Xu, W. Xu, B. Dong, X. Bai, *J. Appl. Phys.* **2011**, *110*, 13611.

[79] X. Y. Huang, X. H. Ji, Q. Y. Zhang, *J. Am. Ceram. Soc.* **2011**, *94*, 833.

[80] Y. Fan, P. Wang, Y. Lu, R. Wang, L. Zhou, X. Zheng, X. Li, J. A. Piper, F. Zhang, *Nat. Nanotechnol.* **2018**, *13*, 941.

[81] W. Zheng, S. Zhou, Z. Chen, P. Hu, Y. Liu, D. Tu, H. Zhu, R. Li, M. Huang, X. Chen, *Angew. Chem.* **2013**, *125*, 6803; *Angew. Chem., Int. Ed.* **2013**, *52*, 6671.

[82] H. B. Beverloo, A. Van Schadewijk, S. Van Gelderen-Boele, H. J. Tanke, *Cytometry* **1990**, *11*, 784.

[83] Y. Liu, S. Zhou, D. Tu, Z. Chen, M. Huang, H. Zhu, E. Ma, X. Chen, *J. Am. Chem. Soc.* **2012**, *134*, 15083.

[84] W. Lv, T. Yang, Q. Yu, Q. Zhao, K. Y. Zhang, H. Liang, S. Liu, F. Li, W. Huang, *Adv. Sci.* **2015**, *2*, 1500107.

[85] M. C. D. Santos, J. Goetz, H. Bartenlian, K. L. Wong, L. J. Charbonniere, N. Hildebrandt, *Bioconjugate Chem.* **2018**, *29*, 1327.

[86] I. Texier, V. Josserand, E. Garanger, J. Razkin, Z. Jin, P. Dumy, M. Favrot, D. Boturyn, J. Coll, *Proc. SPIE* **2005**, *5704*, 16.

[87] H. C. Huang, S. Barua, G. Sharma, S. K. Dey, K. Rege, *J. Controlled Release* **2011**, *155*, 344.

[88] Y. Yang, Q. Zhao, W. Feng, F. Li, *Chem. Rev.* **2013**, *113*, 192.

[89] P. Sarder, D. Maji, S. Achilefu, *Bioconjugate Chem.* **2015**, *26*, 963.

[90] C. N. Keilhauer, F. C. Delori, *Invest. Opthalmol. Visual Sci.* **2006**, *47*, 3556.

[91] B. D. Rosal, D. H. Ortgies, N. Fernández, F. Sanz-Rodríguez, D. Jaque, E. M. Rodríguez, *Adv. Mater.* **2016**, *28*, 10188.

[92] Z. Pan, Y. Y. Lu, F. Liu, *Nat. Mater.* **2012**, *11*, 58.

[93] T. Maldiney, A. Bessière, J. Seguin, E. Teston, S. K. Sharma, B. Viana, A. J. Bos, P. Dorenbos, M. Bessodes, D. Gourier, *Nat. Mater.* **2014**, *13*, 418.

[94] Z. Li, Y. Zhang, X. Wu, L. Huang, D. Li, W. Fan, G. Han, *J. Am. Chem. Soc.* **2015**, *137*, 5304.

[95] A. Abdukayum, J. T. Chen, Q. Zhao, X. P. Yan, *J. Am. Chem. Soc.* **2013**, *135*, 14125.

[96] B. Y. Wu, H. F. Wang, J. T. Chen, X. P. Yan, *J. Am. Chem. Soc.* **2011**, *133*, 686.

[97] N. Li, Y. Li, Y. Han, W. Pan, T. Zhang, B. Tang, *Anal. Chem.* **2014**, *86*, 3924.

[98] N. Li, W. Diao, Y. Han, W. Pan, T. Zhang, B. Tang, *Chem. - Eur. J.* **2014**, *20*, 16488.

[99] B. Y. Wu, X. P. Yan, *Chem. Commun.* **2015**, *51*, 3903.

[100] L. Zhang, J. Lei, J. Liu, F. Ma, H. Ju, *Biomaterials* **2015**, *67*, 323.

[101] A. S. Paterson, B. Raja, V. Mandadi, B. Townsend, M. Lee, A. Buell, B. Vu, J. Brgoch, R. C. Willson, *Lab Chip* **2017**, *17*, 1051.

[102] A. Bessière, S. Jacquart, K. Priolkar, A. Lecointre, B. Viana, D. Gourier, *Opt. Express* **2011**, *19*, 10131.

[103] J. Wang, Q. Ma, X. X. Hu, H. Liu, W. Zheng, X. Chen, Q. Yuan, W. Tan, *ACS Nano* **2017**, *11*, 8010.

[104] X. Qiu, X. Zhu, M. Xu, W. Yuan, W. Feng, F. Li, *ACS Appl. Mater. Interfaces* **2017**, *9*, 32583.

[105] Z. Xue, X. Li, Y. Li, M. Jiang, G. Ren, H. Liu, S. Zeng, J. Hao, *Nanoscale* **2017**, *9*, 7276.

[106] J. Wang, Q. Ma, W. Zheng, H. Liu, C. Yin, F. Wang, X. Chen, Q. Yuan, W. Tan, *ACS Nano* **2017**, *11*, 8185.

[107] Q. Q. Ma, J. Wang, W. Zheng, Q. Wang, Z. H. Li, H. J. Cong, H. J. Liu, X. Y. Chen, Q. Yuan, *Sci. China: Chem.* **2018**, *61*, 1624.

[108] T. Maldiney, A. Lecointre, B. Viana, A. Bessière, M. Bessodes, D. Gourier, C. Richard, D. Scherman, *J. Am. Chem. Soc.* **2011**, *133*, 11810.

[109] Q. L. M. D. Chermont, C. Chanéac, J. Seguin, F. Pellé, S. Maîtrejean, J. P. Jolivet, D. Gourier, M. Bessodes, D. Scherman, *Proc. Natl. Acad. Sci. USA* **2007**, *104*, 9266.

[110] B. Zheng, Y. Bai, H. Chen, H. Pan, W. Ji, X. Gong, X. Wu, H. Wang, J. Chang, *ACS Appl. Mater. Interfaces* **2018**, *10*, 19514.

[111] A. Abdukayum, C. X. Yang, Q. Zhao, J. T. Chen, L. X. Dong, X. P. Yan, *Anal. Chem.* **2014**, *86*, 4096.

[112] J. P. Shi, X. Sun, J. L. Li, H. Z. Man, J. S. Shen, Y. K. Yu, H. W. Zhang, *Biomaterials* **2015**, *37*, 260.

[113] H. Tan, B. Liu, Y. Chen, *ACS Nano* **2012**, *6*, 10505.

[114] B. Liu, C. Sun, Y. Chen, *J. Mater. Chem. B* **2013**, *2*, 1661.

[115] Y. Huang, B. Liu, Q. Shen, X. Zhu, Y. Hao, Z. Chang, F. Xu, P. Qu, M. Xu, *Talanta* **2017**, *164*, 427.

[116] B. Liu, Y. Chen, *Anal. Chem.* **2013**, *85*, 11020.

[117] N. Gao, Y. Zhang, P. Huang, Z. Xiang, F. Y. Wu, L. Mao, *Anal. Chem.* **2018**, *90*, 7004.

[118] W. Sun, J. Yu, R. Deng, Y. Rong, B. Fujimoto, C. Wu, H. Zhang, D. T. Chiu, *Angew. Chem.* **2013**, *43*, 11504; *Angew. Chem., Int. Ed.* **2013**, *52*, 11294.

[119] J. Wu, Z. Ye, G. Wang, D. Jin, J. Yuan, Y. Guan, J. Piper, *J. Mater. Chem.* **2009**, *19*, 1258.

[120] J. Wu, G. Wang, D. Jin, J. Yuan, Y. Guan, J. Piper, *Chem. Commun.* **2008**, *3*, 365.

[121] Q. Li, J. Zhang, W. Sun, J. Yu, C. Wu, W. Qin, D. T. Chiu, *Langmuir* **2014**, *30*, 8607.

[122] W. Yang, L. M. Fu, X. Wen, Y. Liu, Y. Tian, Y. C. Liu, R. C. Han, Z. Y. Gao, T. E. Wang, Y. L. Sha, *Biomaterials* **2016**, *100*, 152.

[123] L. Tian, Z. Dai, L. Zhang, R. Zhang, Z. Ye, J. Wu, D. Jin, J. Yuan, *Nanoscale* **2012**, *4*, 3551.

[124] Z. Ye, M. Tan, G. Wang, J. Yuan, *Talanta* **2005**, *65*, 206.

[125] Y. Chen, Z. Lu, *Anal. Chim. Acta* **2007**, *587*, 180.

[126] C. Song, Z. Ye, G. Wang, D. Jin, J. Yuan, Y. Guan, J. Piper, *Talanta* **2009**, *79*, 103.

[127] H. Jiang, G. Wang, W. Zhang, X. Liu, Z. Ye, D. Jin, J. Yuan, Z. Liu, *J. Fluoresc.* **2010**, *20*, 321.

[128] K. R. Kim, Y. D. Han, H. J. Chun, K. W. Lee, D. K. Hong, K. N. Lee, C. Y. H. , *Biosensors* **2017**, *7*, 48.

[129] Q. X. Wang, S. F. Xue, Z. H. Chen, S. H. Ma, S. Zhang, G. Shi, M. Zhang, *Biosens. Bioelectron.* **2017**, *94*, 388.